UNIVERSITÀ DEGLI STUDI DI NAPOLI
"FEDERICO II"

Scuola Politecnica e delle Scienze di Base

Area Didattica di Scienze Matematiche Fisiche e Naturali

Dipartimento di Fisica "Ettore Pancini"

Laurea Magistrale in Fisica

Astrophysical observables for regular Black Holes

Relatori:
Prof. Mariafelicia De Laurentis
Prof. Piero Nicolini

Candidato:
Giuseppe Filiberto Vitale
Matr. $N94000555$

Anno Accademico 2020/2021

Contents

List of Figures

List of symbols

r_s	Schwrazschild radius
G	gravitational constant equal to $6.67 \times 10^{-11}\, m^3/kg \cdot s^2$
c	speed of light equal to $2.99 \times 10^8\, m/s$
$\hbar$	Planck constant divided by 2π equal to $1.05 \times 10^{-34}\, J \cdot s$
$M_\odot$	solar mass equal to $9.18 \times 10^{37}\, M_P$
M_P	Planck mass equal to $2.17 \times 10^{-8}\, kg$
L_P	Planck length equal to $1.61 \times 10^{-35}\, m$
$g_{\mu\nu}$	metric tensor with two indices that assume the values $\mu, \nu = 0, ..., 3$
x'	derivative of x respect to r
$\dot{x}$	derivative of x respect to affine parameter λ
∇_μ	covariant derivative

Introduction

Quantum Gravity (QG), is the theory that has the attempt to re-conciliate the General Relativity (GR) with the postulates of Quantum Mechanics (QM). Many theories try to resolve this conflict, such as Loop Quantum Gravity, Super-Gravity, Geometrodynamics, String Theory, etc. The principal issue is the non-renormalizability of gravity. From every point of view, Quantum Gravity is related to fundamental length scale where the smooth manifold model of spacetime does not work anymore. The most powerful and intriguing framework to study this theory is the String Theory, where the smallest object, the unit of matter, is the string, which presents some important features such as

- The way the string is excited corresponds to different mass and spin of particles
- The string shares some likeness with black holes when it is highly excited

If we want to analyze more deeply on the small scale such as the Planck scale (L_P), which represents the shortest length-scale of nature in Einstein's gravity [1], we reach energies able to create a black hole. The act of measuring a length shorter than the Planck scale, would require such energy to lead to the formation of a Schwarzschild radius black hole $r_s > L_P$ long before we have any chance to probe the distance itself. From this insight we will show that it is possible to introduce a metric capable to bond the world of particles and black holes.
Not by chance that we focus on studying black holes. This physical system provides a deep link to General Relativity, due to high energy, and Quantum Mechanics, due to the point-like nature of the singularity of space time. Hence, a step forward in physics will be achieved only in these extreme conditions where these two parts of reality are intimately bonded.
Furthermore, the recent advances in astronomy near the event horizons, reached thanks to the Event Horizon Telescope (EHT) collaboration [2]-[3]-[4]-[5]-[6]-[7], allow new constraints on the shadow [8], thanks to analytic arguments as well as numerical calculations, when shortly before it was only possible to test General Relativity for compact binary objects [9]. Due to these progresses, every theory that studies orbits, photon-spheres and shadows of these objects can be analyzed

to show some possible observable deviations from General Relativity .
Coming back, there is an inconsistency between particles and black holes. The problem is that the Compton wavelength of a particle decreases by increasing the mass while the Schwarzschild radius of a black hole increases with its mass. It is possible to conciliate these two aspects considering a suitable energy-stress tensor that takes a natural cut-off in the limit of the Planck scale, in this way a minimum limit is provided both to the Schwarzschild radius and to the minimum sondable length. The last point is the foundation of the UltraViolet (UV) self-complete Quantum Gravity theory. Using a particular metric from this theory [10], it is possible to recover an extremal configuration for a black hole with a length equal to Planck.
But why are extremal configurations so important? Extremal configurations can be descended from the introducing a fundamental length in the line element and can be interpreted as a phenomenological input from Quantum Gravity. It is shown that extremal configuration for black holes suits very well in the UV self-complete scenario providing a stable, minimum size that explores the transition point between particles and black holes. It has been shown that Planck size non-commutative inspired black holes might have been produced during the inflationary state of the Universe [11]. This has some hypothetical phenomenological consequences, such as that extremal black holes turn out to be valid candidates for the dark matter component.
Due to this characteristic, it is possible to circumvent the problem of singularity in a black hole, because everything beneath this scale is meaningless and unsondable.
We will substitute the length of this extremal configuration with an arbitrary parameter. We study the behavior of the resulting case of a static, neutral black hole, the most simple model to observe the behavior of the metric and its consistency. Then we consider some astrophysical observables such as event horizons (EHs), the innermost stable circular orbits (ISCO) of massive particles, the photon orbits (PHS) and eventually the shadows.
Hence, by following the so-called Newman-Janis algorithm, we recover the rotating nature of a black hole with a specific complexification of some parameters [12]. Furthermore, with our metric, we investigate some differences with a Kerr black hole. This will eventually provide corrections to the latter and moreover we may find some constraints that will emerge from these studies.
This thesis is organized as follows:

- In the first Chapter, we introduce a discussion of what black holes are and how we detect them. Furthermore we introduce the UV Quantum Gravity theory that subtend our future considerations and provide us the metric to

use.

- The second Chapter presents the study of a static black hole including event horizons, circular photons and timelike orbits.
- The third Chapter is devoted to the study of a rotating black hole metric, a more realistic case.
- In the fourth Chapter, we will study the shadow for the static case and the rotating case of black holes as L_0 varies.
- Finally, in the conclusions we summarize all the work and we investigate whether and how the deviations can be observed.

Chapter 1

Why Ultraviolet Quantum Gravity metric?

1.1 Introduction to Black Holes

In this Chapter, we will approach the study of the behavior of a black hole with a particular metric, but first of all, it is important to understand why to study a black hole.
A black hole is a region of space-time that has such a strong gravitational field that nothing, neither particles nor light, can escape from it.
These circumstances create the most accurate laboratory to study General Relativity and Quantum Mechanics, the biggest and the smallest description of nature, unfortunately, incompatible each other.
Mainly, the problem is the contrast between the smooth description of the space-time in General Relativity and its oscillations in Quantum Mechanics, due to the Uncertainty principle [13]-[14].
Nowadays Quantum Gravity is the theory that attempts to resolve this conflict with the introduction of a fundamental length which avoids the problem to consider a dimensionless point object. Indeed we can recall one of the most fancy and fascinating theory with this purpose, like the String Theory.
This theory was developed by mistake by Gabriele Veneziano in 1968, when he saw some similarities of data regarding the Strong Nuclear Force with the beta function of Eulero [15]. In 1970 this strangeness was explained with the introduction of an elastic string between particles by Leonard Susskind, and Yochiro Nambu [16]-[17]-[18]-[19]. But it was from the 1974 that theory showed all its potential with the articles of John Schwarz and Joel Scherk [20]-[21]. From a quantum point of view, String Theory predicts the existence of the never observed graviton, the mediator of gravitational force, thanks to the introduction of a very

small vibrating string close to the Planck length ($10^{-33}\mathrm{cm}$). But this is just the beginning; the theory also predicts giant strings, the variable intensity of gravitational force, hidden dimensions, cosmological explanations and other results, the evidences of which are complicated to find with existing technology.
The black holes, which take into account small and large phenomena of reality, provide the perfect background to test String Theory and other theories of Quantum Gravity.
Now we will see the principal features that distinguish them from the other astrophysical objects.

1.1.1 Black hole features

General Relativity predicts that any mass with an adequate small radius can form a black hole, but there are few phenomena in nature that compress the matter spontaneously.
These extreme objects are mostly formed in the life cycle's end of the stars with a mass approximately of $M \sim 3M_{\odot}$ [22]. This seems to be the natural way to form a black hole, at least for the stellar-mass ones.
The process begins when the nuclear reactions, which merge all the nucleus of the soft atoms from the hydrogen to steel in the stars, are not enough to resist gravitational force. Besides the stellar-mass black hole, it is estimated that, at the centre of the majority of the galaxies, there are supermassive black holes of millions of solar masses, but they are not the only ones. We will divide them into categories, but now we see their properties.
Some features are in common with all the black holes [22].
In the outermost part of a black hole, the matter in the vicinity of a black hole is so heated, by the friction of its strength, that it forms a region called "accretion disk" formed by diffuse material in orbital motion around it. The matter in unstable orbits will spiral towards the central body increasing the total mass of the black hole.
The matter, before falling into the center of the black hole, passes through a boundary called "event horizon". This region is described as the boundary of the black hole within which the escape velocity is greater than the speed of light, beyond which it is impossible to go back. It is literally a point of no return and it is the first 'apparent' singularity that an object encounters towards the center of the black hole.
At the center of the black hole, the General Relativity predicts a "singularity" where all the laws of physics break down. The energy density is infinite and this suggests that the theory is no longer valid to describe a black hole at those scales.
After a first generic description, let us now study black holes in more detail.
In general, the black holes have to respect the No-Hair theorem that states that

they can be described by only three externally observable classical parameters (for this reason we say that they have 'no hair') : mass M, electric charge Q, and angular momentum J, that follow the relation

$$M^2 - \left(J^2/M^2\right) - Q^2 \geq 0$$

where $G = c = 1$. For the parameters that obey this relation we have a unique solution of black hole for Einstein-Maxwell equations.
The first exact solution have been developed in 1916 by K. Schwarzschild [23]. It is about the study of Einstein's equations of a static symmetrical body in vacuum. Only the mass, of the three parameters that define a black hole, has been considered in the solution.
We introduce a metric tensor $g_{\mu\nu}$ which defines the notions of distance, angle and curvature, so describes how space-time changes due to the presence of an object. Explicitly Schwarzschild metric can be written in spherical coordinates as

$$ds^2 = \left(1 - \frac{2GM}{c^2 r}\right) c^2 dt^2 - \left(1 - \frac{2GM}{c^2 r}\right)^{-1} dr^2 - r^2 d\theta^2 - r^2 sin^2\theta d\phi^2$$

Where G is the gravitational constant, c is the speed of light and M is the mass of the considered object. This solution is singular in $r = 0$, where we have the so-called singularity, but it also contains an 'apparent' singularity in $r = r_s$, where we have the event horizon at the Schwarzschild radius $r_s = 2GM/c^2$ derived for $g_{tt} = g_{rr}^{-1} = 0$.
The event horizon is an apparent singularity because, with an adequate coordinate system called Eddington-Finkelstein coordinates [24], we can observe how it is traversable, reducing the singularity only to a problem of choice of the reference system. This exact solution is a useful approximation to study slowly spinning black holes, but unfortunately, real black holes are rotating, so we have to use another more complicated solution.
Indeed, in this case we have to introduce also a rotation parameter of the black hole describing its angular momentum. For this reason we use another solution developed by R. P. Kerr in 1963 [25], which represents the most realistic case. It describes the geometry of an axially-symmetric black hole, and it is also an exact solution of the Einstein equations despite its very highly non linear form. The Kerr metric describes the geometry of space-time in the vicinity of a mass M rotating with angular momentum J. We write it in Boyer-Lindquist coordinates, which represent a generalization of the coordinates used for the metric of a Schwarzschild black hole. The metric has the following form

$$ds^2 = -\left(1 - \frac{2Mr}{\Sigma}\right)dt^2 - \frac{4Mrasin^2\theta}{\Sigma}dtd\phi + \frac{Asin^2\theta}{\Sigma}d\phi^2 + \frac{\Sigma}{\Delta}dr^2 + \Sigma d\theta^2$$

The coordinates r, θ and ϕ are standard oblate spheroidal coordinates.
Here it was considered $G = c = 1,\ \Sigma = r^2 + a^2cos^2\theta,\ \Delta = r^2 - 2Mr + a^2$ and $A = (r^2 + a^2)^2 - \Delta a^2 sin^2\theta$, where M is the mass and a is the rotation parameter linked to the angular momentum as $J = aM$.
In addition to the central singularity for $r = 0$, unlike the case of Schwarzschild metric, we have two event horizons, derived by $g_{tt} = g_{rr}^{-1} = 0$, for

$$r_- = \frac{r_s + \sqrt{r_s^2 - 4a^2}}{2} \qquad\qquad r_+ = \frac{r_s + \sqrt{r_s^2 - 4a^2cos^2\theta}}{2}$$

we can see how the horizons of events touch each other at the poles for $\theta = \pi/2$.
The region between these two surfaces is called "ergosphere". This region is literally a vortex of the space-time. The matter, in this region, has the possibility to escape from the ergosphere, because it is still outside the inner event horizon but it cannot escape radially because of the strength of the vortex inside the outer event horizon.
If we want to include also the electric charge, in that case we use the Kerr-Newman solution [26].
This is the way we can infer the gravitational field of the black holes in the General Relativity. But that is not enough, the theory cannot explain problems such as those relating to the central singularity.
For this issue, it is considered that an efficient model for their explanation will be only an adequate theory that also accounts for Quantum Mechanics because of the point-like nature of the singularity, i.e. Quantum Gravity.
A theory, which also fully includes Quantum Mechanics in General Relativity, will provide more explanations than now.
When we account for Quantum Mechanics, even at a basic level, something strange happens as S. Hawking found out in 1975 [27]. Before that, a black hole was thought to be eternal, but later we realized that it actually evaporated with the so called Hawking radiation. The idea is that, from the vacuum of space, pairs of particles are created, but near the event horizon, some can escape from it forming an emission when their partners are trapped in it.
The debt in energy for the void is paid by the black hole that decreases its mass

increasing its temperature. This process is inversely proportional to the mass and the effect time for a common black hole is more larger than the age of the entire Universe.

1.1.2 Mass, a first discriminant

Now, we will list the main classes of black holes we know about. There are principally four types of black holes, divided by mass and formation [22]:

- Stellar-mass black holes are the most understood of this kind, they are generated by the collapsing of a massive star approximately between $\sim 3M_\odot$ and $\sim 30M_\odot$. The lower limit is given by the Tolman-Oppenheimer-Volkoff limit, which give an upper bound to the mass of cold, non-rotating neutron stars. If the mass of the collapsing core of the star is larger of this limit, one expects a formation of a black hole.

- Intermediate-mass black holes , as the name suggests, lie between stellar-mass and supermassive black holes. They have been observed from $\sim 60M_\odot$ to $\sim 130M_\odot$, also if they are usually defined as black holes with a mass of up to $10^5 M_\odot$ [28]. They are formed by the merging of various stellar-mass black hole.

- Supermassive black holes are giant of their kind, they overpass $10^5 M_\odot$ and there are only theories for their genesis. Their formation is thought to be due to the fusion chain of black holes and stars, but their origin is mostly unknown.
  Their core incorporate more and more material from the outside until they eventually are collocated at the centre of the galaxies, such as Sagittarius A at the centre of the Milky Way (our galaxy) with a mass of $4 \times 10^6 M_\odot$ or M87 at the centre of Virgo cluster with a mass of $6,6 \times 10^9 M_\odot$ [7]. The latter is the first black hole directly observed in 2019 by the EHT [2]-[7].

- Primordial black holes, they are only hypothetical and were probably born at the beginning of the Universe, in the first second after the Big Bang, when the Universe was not yet homogeneous and some parts of the space-time were rich in energy. They have a mass up to $\sim M_\odot$ and can be a possible explanation to supermassive black holes. There is a lower limit in mass in order that the Hawking radiation allows their existence. It can be estimated that black holes with a mass of about $\sim 5 \times 10^{14} g$ would not resist until now.

1.1.3 How to detect them?

There are some indirect ways to see them, here we list some of.
Because of their gravitational strength, the black holes influence the matter in their vicinity, forcing it to warm up until huge temperatures. So, the emission of particles at great intensity is the first sign of the presence of a black hole. This emission lies in the spectrum of the X-rays. Unfortunately, the atmosphere is a wall for this interval, but thanks to telescopes in orbit, it is possible to detect them. In this way, we have detected a binary system of a black hole and a companion star, Cygnus X-1 [29], composed of a supergiant blue star and a stellar mass black hole of $\sim 14,8 M_{\odot}$ according to the last estimates [30]. The latter was the first indirect evidence of a black hole in 1971.
Another suspicion of their presence is due to the orbits of the stars around a gravitational center and the lensing effect that produces multiple images in the Celestial sphere [31]. From their orbits it is possible to recover the mass of the gravitational centre. If the mass exceeds three solar masses, it is likely the presence of a black hole.
In the end, there is the study of the gravitational waves. They are formed when two or more black holes are merging each other. This movement is so violent that the space-time is altered because of their increasing orbital velocity to the apex of the merging, producing gravitational waves such as those detected from LIGO and Virgo collaborations in 2016 [32].
LIGO and Virgo [33]-[34] are huge observatories respectively of 4 km and 3 km, L-shaped, situated in Louisiana, Washington and Pisa. The technology of the observatories is based on laser interferometry of Michelson in which there are two arms with two laser beams inside, in the infrared, which interfere. When a gravitational wave is detected, there is a phase displacement that produces a signal. In 2016 we have observed for the first time the merger of two stellar-mass black holes, one of $\sim 29 M_{\odot}$ and the other of $\sim 36 M_{\odot}$.
Thanks to the increase of the technology, now it is possible also to see directly the image of a black hole.
It was in 2019 that Event Horizon Telescope [3] announced the first image of M87, a supermassive black hole in the Virgo constellation. It is the most large telescope in humanity's history, and it uses very-long-baseline interferometry (VLBI) stations around Earth.
The dimension of this virtual telescope is large as the Earth, and operates at the nominal operating wavelength of $\lambda \sim 1.3\, mm$ with an angular resolution of $\lambda/D \sim 25\, \mu as$, where D is the virtual telescope's diameter.
In the future, the aim of the collaboration is to improve the data reducing the observational wavelength and so the angular resolution.
This is the wavelength where the EHT is well established to observe the imme-

diate nearby of the black holes. The shorter are the observable wavelengths, the more challenging are the difficulties due to noise in electronics and the decreased efficiency of radio telescopes [2]. The angular resolution has reached such a degree of sensitivity, that for comparison, is the same as observing of one of the dimples of a golf ball in Los Angeles from New York.
Every day the possibility to test Quantum Gravity theories in the details is becoming ever and ever more solid and Sagittarius A will be soon the next to observe, providing us to have a further way to discriminate the various theories emerging.
Comforted by the increase of these technologies, we approach the study of the Ultraviolet Quantum Gravity.

1.2 Ultraviolet Quantum Gravity

This chapter aims to introduce an appropriate metric to study a case in which there is a fundamental length, the Planck scale, which we consider as the length of a black hole's extremal configuration.
We want to use the Ultraviolet (UV) Quantum Gravity because it provides a solution for the problem of the black hole's singularity, as it provides a wall to observations in the Planckian and sub-Planckian length scale, as mentioned above in the Introduction, making it unnecessary to ask what happens to the scales of a singularity.
This is the foundation for some further generalizations, such as the use of an arbitrary scale for the extremal configuration as we will do. This argument is largely based on the paper [10] which is the framework of this work.

1.3 From energy density to metric

In this section we look for a metric that takes into account the transition from particles and black holes.
Building step by step a tensor with all the features of interest, we search an adequate form for energy density of Einstein's equations. This particular tensor allows for passages between particle-like objects and black holes, as UV self-complete Quantum Gravity requires (Figure 1.3) to get a consistent metric.
The general energy density for a point-particle in spherical coordinates is

$$\rho_r = \frac{M}{4\pi r^2}\frac{d}{dr}\theta(r) \tag{1.1}$$

The energy distribution (1.1) in this form, for the moment, implies a black hole for

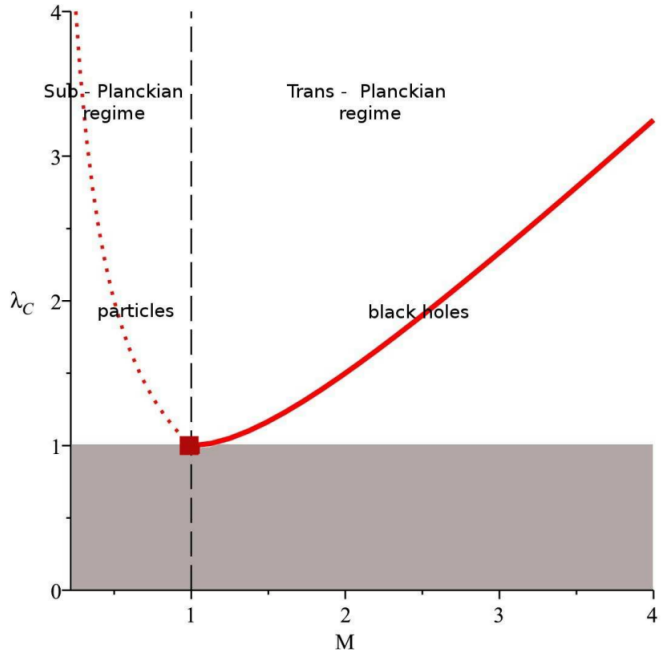

Figure 1.1: This shows a plot of length in function of energy. Particles (dotted line) and black holes (solid line) cannot probe length shorter than the Planck length, the area represented by a grey box. This picture is taken in P. Nicolini and E. Spallucci [10], see Figure 1 there

every value of mass M, also for values under the Planck scale where we expect just particles. $\theta(r)$ is the function of Heaviside tied to delta Dirac as

$$\delta(r) = \frac{d}{dr}\theta(r) \tag{1.2}$$

Particles and black holes can be accounted for by modifying the energy distribution acceptably, such as to tame the ambiguities of the Schwarzschild metric in the near-Planckian regimes. This can be achieved by considering a smooth function $h(r)$ instead of the Heaviside step

$$\theta(r) \to h(r) \tag{1.3}$$

Then the new energy density becomes

$$\rho_r = \frac{M}{4\pi r^2}\frac{d}{dr}h(r) \equiv T_0^0 \tag{1.4}$$

The other components of the stress tensor are determined from the conservation equation $\nabla_\mu T^{\mu\nu} = 0$ which turns out to be of the form

$$T^\mu_\nu = diag(-\rho, p_r, p_\perp, p_\perp) \tag{1.5}$$

Where p_r is obtained from the equation of state $-\rho = p_r$ and the angular pressure is specified by the conservation of the stress tensor $p_\perp = p_r + \frac{r}{2}\partial r p_r$. By inserting the tensor in Einstein equations, one finds that the metric is (for $G = 1$)

$$ds^2 = -\left(1 - \frac{2m(r)}{r}\right) dt^2 + \left(1 - \frac{2m(r)}{r}\right)^{-1} dr^2 + r^2 d\Omega^2 \tag{1.6}$$

with

$$m(r) = 4\pi \int^r dr' (r')^2 \rho(r') \tag{1.7}$$

We can see that some properties are fulfilled such as that at large distances $r >> L_P$, the above energy density has to vanish in order to preserve the vacuum case of Schwarzschild metric. Conversely, at shorter distances $r \sim L_P$, the density $\rho(r)$ (and accordingly $h(r)$) has to fulfil the following requirements:

- No curvature singularity in the core;
- Self-implementation of a characteristic scale l_0 equal to the extremal configuration r_0 ;

the aim is just to use r_0 as fundamental scale, not considering of any l_0 that comes out from any theory not arising from Einstein field equations. Since there is nothing beyond Planck Scale providing us a natural limit, we setting $r_0 = L_P$.
In this way it is achieved the first requirement and implemented the second condition. At this point, the resulting extremal black hole is just the smallest object one can use as unity of distance in physics. In this way, for the UV self-complete Quantum Gravity, it is not physically meaningful to ask about curvature singularity inside the horizon because the spacetime that we consider is no longer defined below this length scale. The most natural choice for $h(r)$ it is then

$$h(r) = 1 - \frac{L_P^2}{r^2 + L_P^2} \tag{1.8}$$

and substituting this in (1.1), it is obtained the quantity

$$\rho(r) = \frac{M}{2\pi r} \frac{L_P^2}{\left(r^2 + L_P^2\right)^2} \tag{1.9}$$

finding the following metric that models a particle-black hole system

$$ds^2 = -\left(1 - \frac{2ML_P^2 r}{r^2 + L_P^2}\right) dt^2 + \left(1 - \frac{2ML_P^2 r}{r^2 + L_P^2}\right)^{-1} dr^2 + r^2 d\Omega^2 \tag{1.10}$$

where M is defined as

$$M = \frac{1}{2L_P^2 r_h} \left(r_h^2 + L_P^2\right) \tag{1.11}$$

M has the physical meaning of mass for a spherical, holographic screen with radius r_h.
In the framework of this theory, the physics in three-dimensional space can be projected on a two-dimensional "viewing screen" with no loss of information [35]. There are some intriguing arguments on behalf of holographic theory, such as the question that the the maximum entropy is proportional to the area and not to the volume of the region [36] and the question that the dynamic of the three dimensional space can be projected in a "viewing screen", a large region that represents the boundary of our Universe that can be regarded to be a flat space at infinity [37].
Some remarks are worth to see for this metric such as that we have $M = M_P$ only if $r_h = L_P$ and that the metric (1.10) admits a pair of horizons given from

$$r_\pm = L_P^2 \left(M \pm \sqrt{M^2 - M_P^2}\right) \tag{1.12}$$

For $M = M_P$ the two horizons meet each other in $r_\pm = r_0 = L_P$. For $M >> M_P$ the outer horizon approaches the shape of the Schwarzschild case.

Chapter 2

Static case "Schwarzschild like"

In this Chapter, as ground for the development of the work, we take the UV metric and substitute the Planck length L_P with a free parameter L_0, in this way it is provided an extremal configuration no more fixed.
The behavior of a black hole emerging from this metric will be the subject of this thesis.
Then we analyze the resulting horizons and photonspheres to run the parameter L_0 for the static case [38]. These quantities will be more closely probed thanks also due to recent advances in gravitational waves astronomy, besides EHT [2]-[7], we can see a development on data from LIGO collaboration [39] and from LISA collaboration [40].
Hence, there is a chance that can be possible to distinguish between near-horizons physics of classical black hole and potentially astrophysical mimickers.

2.1 Event Horizon

Taken the following metric

$$ds^2 = -\left(1 - \frac{2MGr}{r^2 + L_0^2}\right) dt^2 + \left(1 - \frac{2MGr}{r^2 + L_0^2}\right)^{-1} dr^2 + r^2 d\Omega^2 \tag{2.1}$$

where $G = L_P^2$, $\hbar = 1$, $c = 1$ and M is defined as

$$M = \frac{1}{2L_0^2 G r_h} \left(r_h^2 + L_0^2\right) \tag{2.2}$$

L_0 represents our fundamental length, and in this case, the deviation from the Schwarzschild metric.

(Note that for $L_0 = 0$, Schwarzschild metric is recovered, for $L_0 = L_P$ we can recover the metric (1.10)).
It is possible to obtain the event horizons from the identity

$$g_{tt} = 1 - \frac{2MGr}{r^2 + L_0^2} = 0 \tag{2.3}$$

Before to continue, we can see how to re-normalize this equation to introduce some unit of measure. Since $G = L_P^2$, we can write all in function of Planck's mass and length.

$$= 1 - \frac{2(ML_P)(rL_P)}{\frac{L_P^2}{L_P^2}(r^2 + L_0^2)} = 0$$

$$= 1 - \frac{2(M/M_P)(r/L_P)}{(r/L_P)^2 + (L_0/L_P)^2} = 0 \tag{2.4}$$

$$= 1 - \frac{2M(M_P)r(L_P)}{r^2(L_P) + L_0^2(L_P)} = 0$$

Considering that $M_P \sim 10^{-38} M_\odot$ and that $L_P \sim 10^{-38} km$ we can write indistinctly also in these new units

$$g_{tt} = 1 - \frac{2M(M_\odot)r(km)}{r^2(km) + L_0^2(km)} = 0 \tag{2.5}$$

Adimensionally we have the solution

$$r^2 + L_0^2 - 2Mr = 0 \tag{2.6}$$

Plotting before the plots with M fixed and then those with L_0 fixed, we can see the difference for different unit of measures

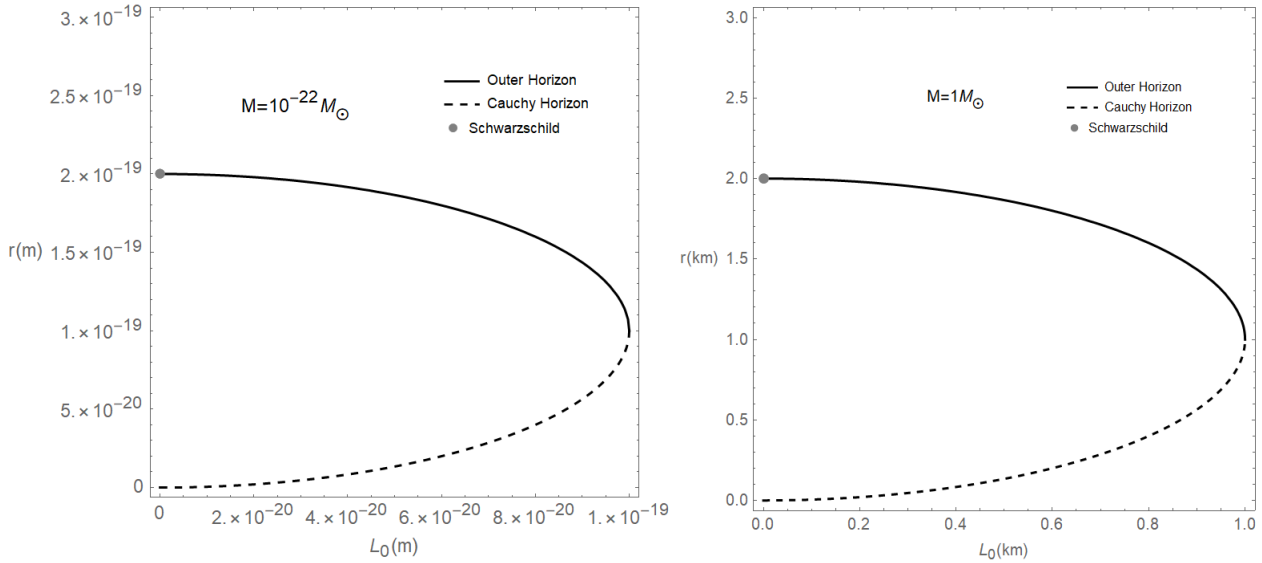

Figure 2.1: In black line is represented the outer horizon, in black dotted line the Cauchy horizon, in gray point and line the Schwarzschild horizon. They are plotted as r versus the free parameter L_0 while $M = 10^{-22}M_\odot$ and $M = 1M_\odot$ above and as r versus the parameter M while $L = 10^{16}L_P$ and $L = 1L_P$ below.

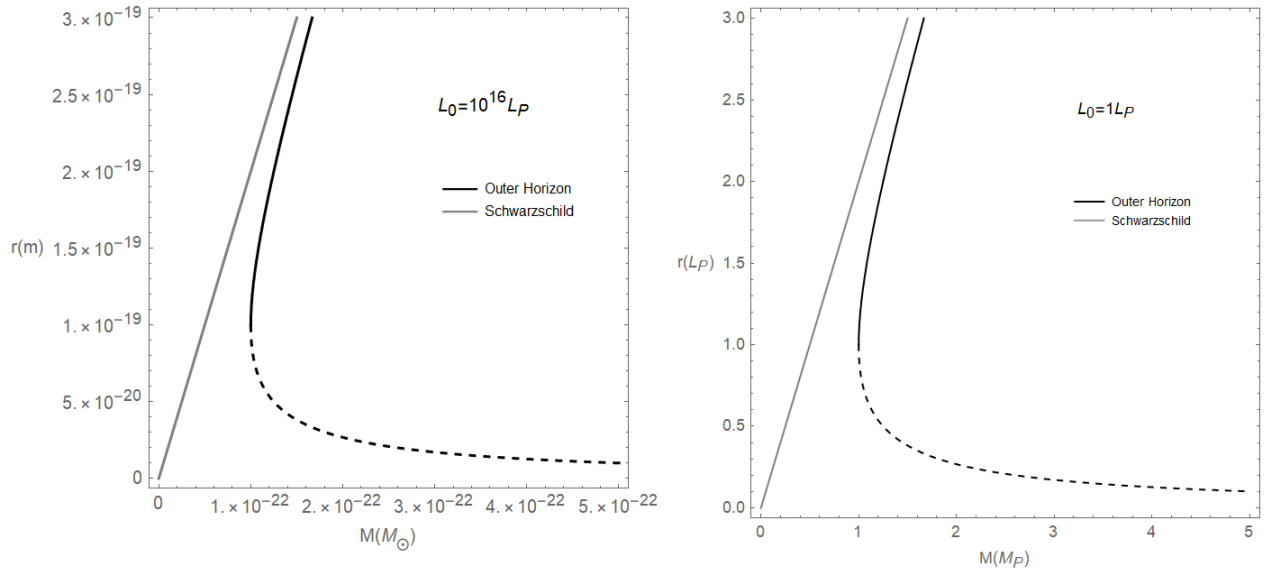

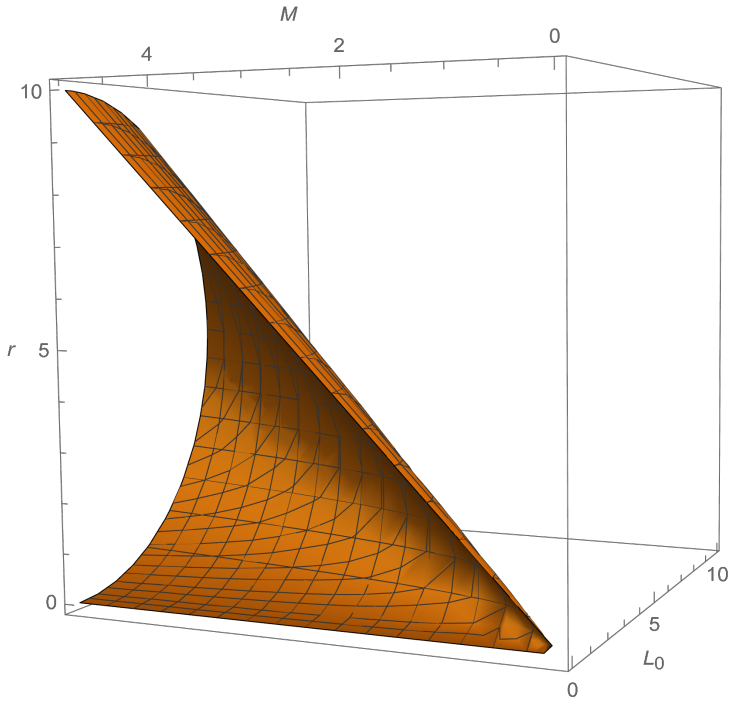

Figure 2.2: Here is shown the behavior of the horizons when all the three parameters are free and adimensional for an $M = 5$

From these graphs we can see that the longer the fundamental length L_0 the longer is the deviation from the static case reached for $L_0 = 0$.
The maximum of L_0 is provided from the maximum of M since $0 < L_0 < M$.
We have seen also the case of $10^{16} L_P = 10^{-19} m$, the minimum distance reached from LHC with an energy of $\sim 14\, TeV$ [41]. This distance can be deduced by the formula of photon's energy

$$E = h\nu = h\left(\frac{c}{\lambda}\right) \longrightarrow \lambda = \frac{hc}{E} \tag{2.7}$$

where we obtain a value of the minimum distance investigated of $\sim 10^{16} L_P$.
In this case we can see that the maximum difference from the static case, for a mass of $10^{16} M_P = 10^{-22} M_\odot$, is only of $10^{16} L_P = 10^{-19} m$.

2.2 Effective Potential

For the study of photonsphere is useful to start from the vector tangent to world-line for a massive and a massless particle [38].

$$g_{\mu\nu}\frac{dx^\mu}{d\lambda}\frac{dx^\nu}{d\lambda} = -\left(1-\frac{2Mr}{r^2+L_0^2}\right)\left(\frac{dt}{d\lambda}\right)^2+\left(1-\frac{2Mr}{r^2+L_0^2}\right)^{-1}\left(\frac{dr}{d\lambda}\right)^2+r^2\left(\frac{d\Omega}{d\lambda}\right)^2 = \epsilon$$

where $\epsilon \in \{-1, 0\}$, -1 corresponds to massive particle while 0 corresponds to massless particle.
Thanks to the presence of the time and the angular Killing vector, we can define the quantities

$$E = \left(1-\frac{2Mr}{r^2+L_0^2}\right)\frac{dt}{d\lambda} \qquad\qquad L = r^2\frac{d\phi}{d\lambda} \tag{2.8}$$

corresponding to the energy and the angular momentum of the particle. Substituting them in (2.2) we obtain

$$E^2 = \left(\frac{dr}{d\lambda}\right)^2 + \left(1-\frac{2Mr}{r^2+L_0^2}\right)\left(\frac{L^2}{r^2}-\epsilon\right) \tag{2.9}$$

If we set up the metric with $\theta = \pi/2$. We can identify an *effective potential* for geodesic orbits

$$V_\epsilon = \left(1-\frac{2Mr}{r^2+L_0^2}\right)\left(\frac{L^2}{r^2}-\epsilon\right) \tag{2.10}$$

2.3 Existence of Photonsphere

For photonsphere orbits we can set $\epsilon = 0$ and get

$$V_0 = \left(1-\frac{2Mr}{r^2+L_0^2}\right)\frac{L^2}{r^2} \tag{2.11}$$

Since for $dr/d\lambda = 0$ we have some turning points, a minimum for V_0 can give the circular orbit for a massless particle. So we study the first derivative of an

effective potential

$$V_0' = \frac{2L^2(L_0^4 + r^3(r-3M) + L_0^2 r(2r-M))}{r^3(L_0^2+r^2)^2} \tag{2.12}$$

the location of a circular photon orbit, is given implicitly by the equation

$$L_0^4 + r^3(r-3M) + L_0^2 r(2r-M) = 0 \tag{2.13}$$

Rewritten before for M fixed and then with L_0 fixed, it provides for the following plots:

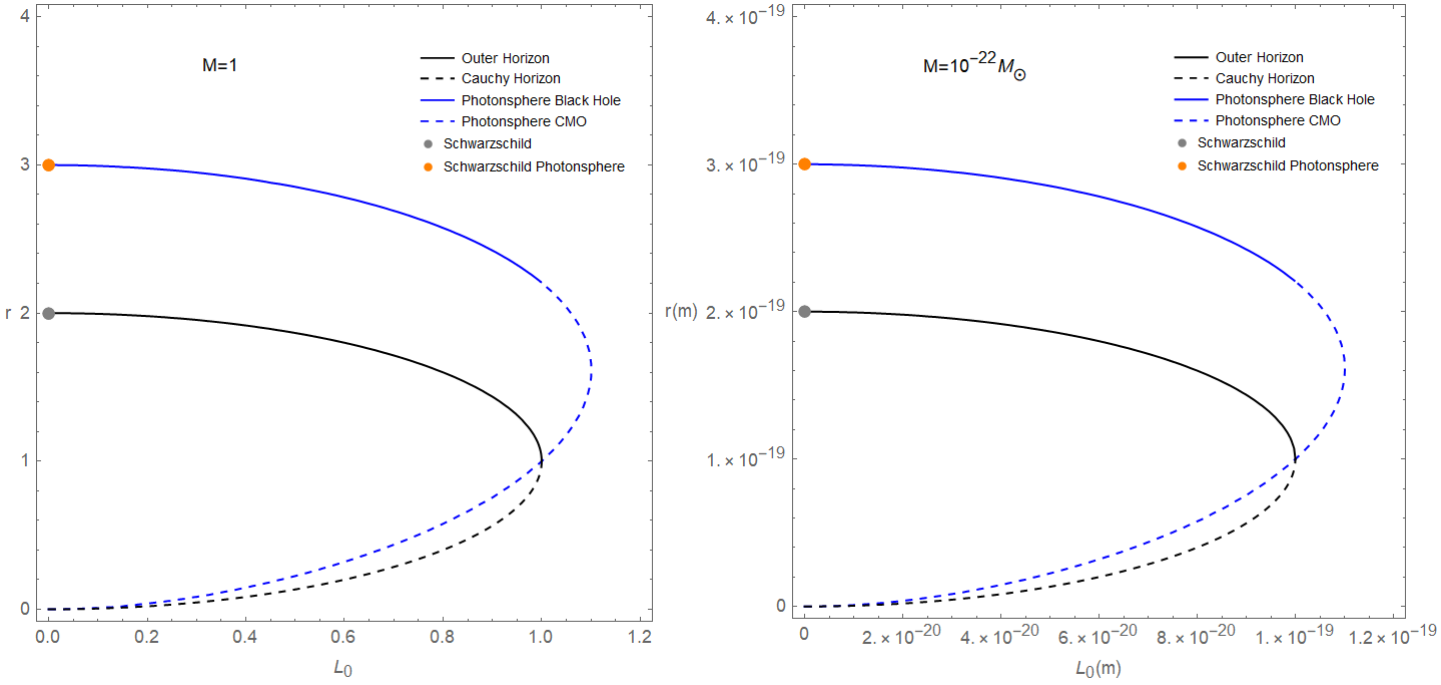

Figure 2.3: In black line is represented the outer horizon, in black dotted line the Cauchy horizon, in gray Schwarzschild horizon, in orange the Schwarzschild photonsphere, in blue line the photonsphere, in blue dotted line the photonsphere of CMOs. Above we have the adimensional graphic for $M = 1$ and the case of $M = 10^{-22}M_\odot$ in function of L_0, below we have the adimensional graphic for $L_0 = 1$ and the case of $L = 10^{16}L_P$ in function of M

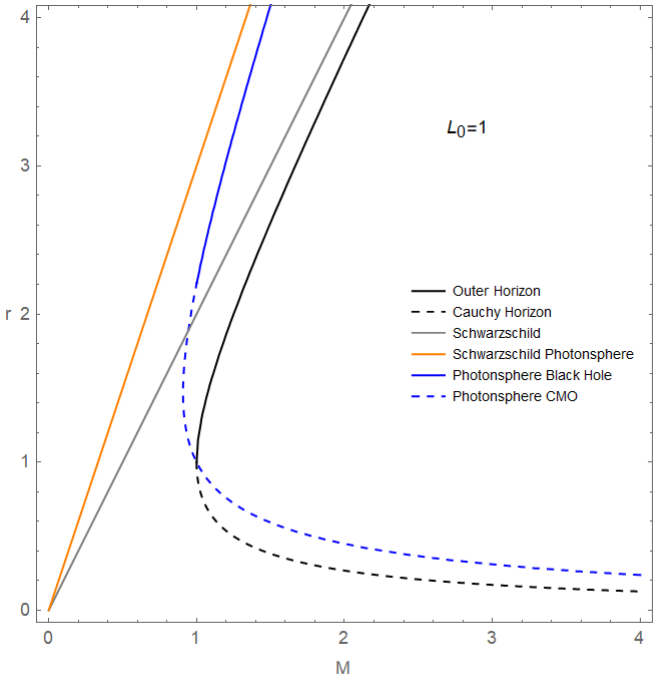

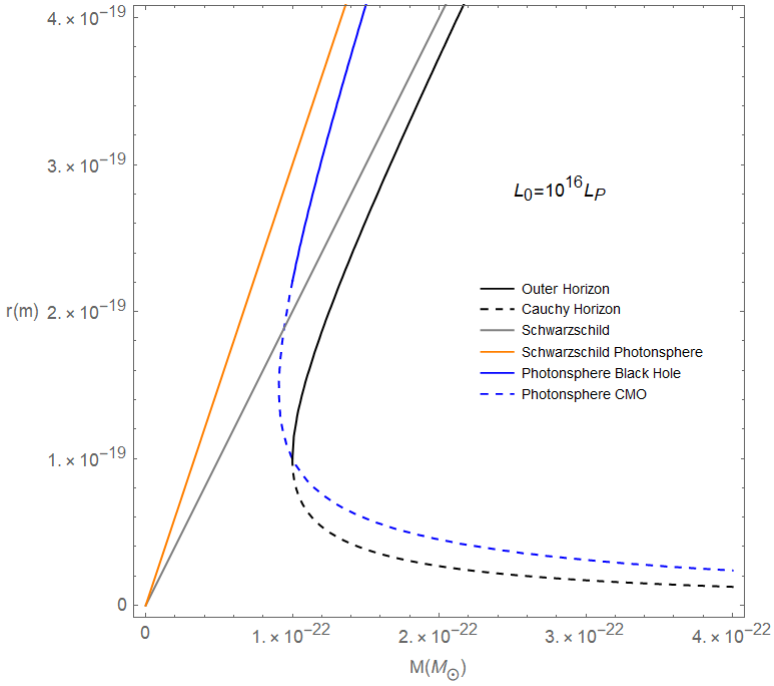

It is possible to identify the region of existence of the photonsphere for $r > 1$, from the point where there is the encounter of photonsphere and event horizon. It is possible to discriminate also the *Compact Massive Objects* (CMOs) for $L_0 > 1$ e $M < 1$.
For $L_0 = 1$, we have compact massive objects for $0.9083 < M < 1$.
For example, in the dimensional case, if $L_0 = 10^{16} L_P$, we can have CMOs for a range between $0.9083 \times 10^{-22} M_\odot < M < 10^{-22} M_\odot$.
Furthermore we can see that also in this case for $L_0 = 0$, we recover the photonsphere of the static case.

2.4 Stability and Instability of photon orbit

To control the stability of the circular orbits for null trajectories we have to study the second derivative of the effective potential

$$V_0'' = \frac{2L^2(3L_0^6 + 3r^5(-4M + r) + L_0^4 r(-2M + 9r) + L_0^2(-6Mr^3 + 9r^4))}{r^4(L_0^2 + r^2)^3} \tag{2.14}$$

We can check that for circular photon orbits, in the case which $M = 1$ we have $V_0'' < 0$ for value $L_0 < 1.10091....$ Substituting this value in (2.13) it obtains

$r_{ph} = 1.61603...$ so we have that for the point $(r_{ph}, L_0) \simeq (1.61603..., 1.10091...)$ that $V_0'' = 0$.
Hence, we have *existence* and *instability* in the region $r_{ph} \in (1, 1.61603...)$ and *existence* and *stability* in $r_{ph} \in (1.61603..., \infty)$.

2.5 Timelike circular orbits

For these orbits we have to come back to the effective potential (2.10), and substitute $\epsilon = -1$. In this way we consider all massive particles

$$V_{-1} = \left(1 - \frac{2Mr}{r^2 + L_0^2}\right)\left(\frac{L^2}{r^2} + 1\right) \tag{2.15}$$

As done for the massless case, we have to study the first derivative to put equal to 0

$$V_{-1}' = -\frac{2\left(L_0^4 L^2 - Mr^5 + L_0^2\left(Mr^3 + L^2 r(2r - M)\right) + L^2 r^3(r - 3M)\right)}{r^3\left(L_0^2 + r^2\right)^2} \tag{2.16}$$

So all the timelike circular orbits have to satisfy the following equation

$$L_0^4 L^2 - Mr^5 + L_0^2\left(Mr^3 + L^2 r(2r - M)\right) + L^2 r^3(r - 3M) = 0 \tag{2.17}$$

From a physical point of view, we require that $0 \leq L^2 < \infty$, so we get the angular momentum

$$L^2 = \frac{Mr^5 - L_0^2 Mr^3}{r^4 - 3Mr^3 + 2L_0^2 r^2 - L_0^2 Mr + L_0^4} \tag{2.18}$$

Now it is possible matching all the values of L^2 with the previous plots

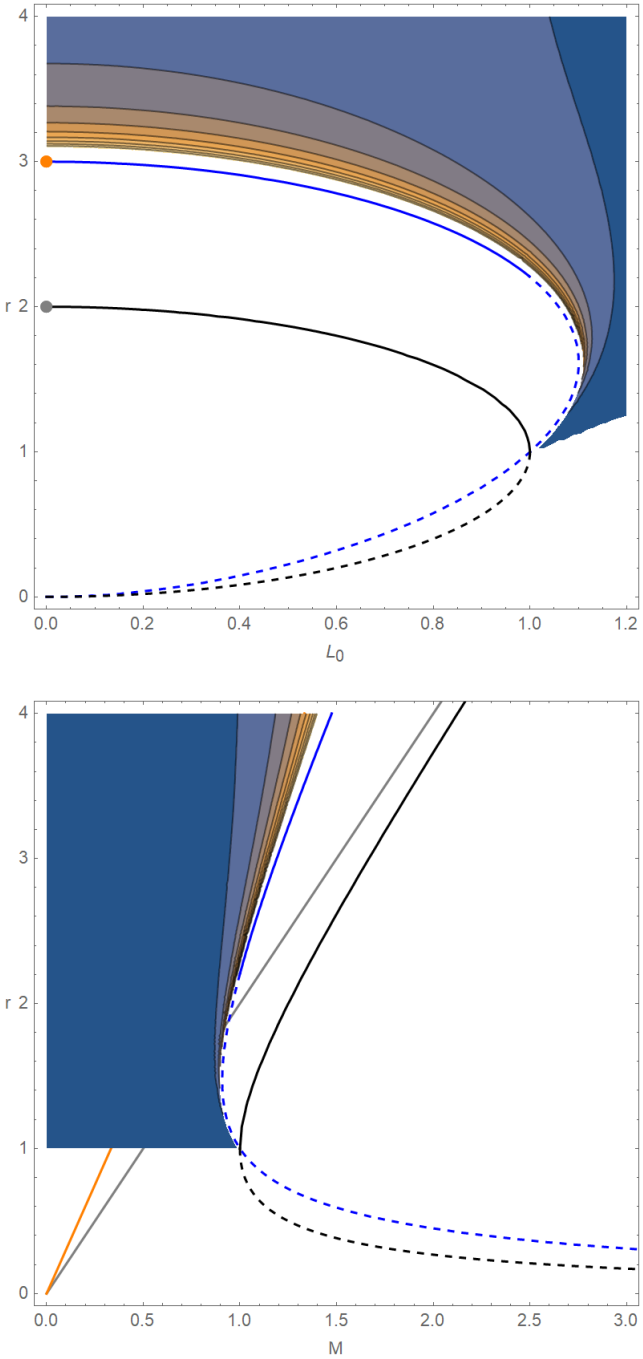

Figure 2.4: In black line is represented the outer horizon, in black dotted line the Cauchy horizon, in gray line the Schwarzschild horizon, in orange line the Schwarzschild photonsphere, in blue line the photonsphere, in blue dotted line the photonsphere of CMOs. It is represented the time like orbits as L^2 changes, the above plot for $M = 1$, that below for $L_0 = 1$

Chapter 3

Rotating metric with Newman-Janis Algorithm

Completed the study of the static case, we demand what happens if we investigate the more realistic case of the rotating metric and, to do it, we can use an algorithm called of Newman-Janis. The Newman-Janis algorithm (NJA for simplicity) is a procedure to obtain a rotating metric from a non rotating one. Despite its simplicity, it is not quite clear why it is so successful. After the original discovery of the Kerr metric [25], Newman and Janis [42] showed that this solution could be derived by making an elementary complex transformation to the Schwarzschild solution. In this way it was been derived also the solution for a rotating and charged black hole from the Reissner-Nordstrom metric.
There is such a debate on the functioning of this algorithm that seems very successful for exterior solutions but not the same one can say for the interior ones. We can recall such attempts for example in the work of S. P. Drake and R. Turolla [43], where they were searching an interior metric that could be matched smoothly with the exterior one but with some lack on an acceptable physically reasonable seed metric; or in the work of Stefano Viaggiu [44] where starting from the Schwarzschild solution, he recovers the interior Kerr solution with the application of the NJA and where he studies the slowly rotating limit.
The issue of not finding an acceptable interior solution reflects the fact to find a physically reasonable source for the Kerr solution due to the several restrictions to impose, among the most important, the fact that it has to be a non radiating source and moreover, in the limit of the static case, it has to recover the interior Schwarzschild solution.
Although the perfect fluid source is the most natural choice, it seems that an anisotropic source it is a reasonable candidate for the interior solution at least for an oblate spheroid in Kerr metric until to the fifth grade of a perturbative parameter as shown in the work of P. Florides [45]. Nevertheless this does not implicate

that a perfect fluid it cannot be found at all.
Hence, the study of the consistencies between the exterior and interior solution is very important to provide a generalization of the algorithm and also a reason to why it is so successful. This lack of a generalization is also a reason to why the NJA is not working in some theories as for instance in rotating Dilaton-axion Black Hole and BraneWorld in the work of R. Canonico, L. Parisi and G. Vilasi [46].
Although its imperfections, NJA is a very powerful tool to get a rotating geometry. According to [47] the particular choice of the complexification used in the standard NJA to generate the Kerr-Newman solution are not arbitrary, but in fact could be chosen in no other way in order for the NJA to be successful at all. This provides a sense on the use of the algorithm.
In this work we do not focus on the why NJA works, but we will introduce a general procedure for it in section 1 and the consecutive application to our metric in section 2. Then we will approach the study of event horizons (EHs) and photonsphere (PHS) of this new rotating metric in section 3 and 4.

3.1 Four steps for Newman-Janis Algorithm

We treat the NJA as a four-step procedure to generate new solutions of Einstein's equations from a general static spherically symmetric body. In the following it is presented the procedure:

- We start from a symmetric line element [48]:

$$\begin{aligned} ds^2 &= e^{2\phi(r)}dt^2 - e^{2\lambda(r)}dr^2 - H(r)d\Omega^2 \\ &= G(r)dt^2 - \frac{dr^2}{F(r)} - H(r)d\Omega^2 \end{aligned} \tag{3.1}$$

  Using the Eddington-Finkelstein coordinates u, r, θ, ϕ, where

$$u = t - r* \tag{3.2}$$

  and $dr* = dr/\sqrt{GF}$, the above line element can be written as

$$ds^2 = G(r)du^2 + \sqrt{\frac{G(r)}{F(r)}}dudr - H(r)d\Omega^2 \tag{3.3}$$

- Express the contravariant form of the metric in terms of a null tetrad

$$g^{\mu\nu} = l^{\mu}n^{\nu} + l^{\nu}n^{\mu} - m^{\mu}\bar{m}^{\nu} - m^{\nu}\bar{m}^{\mu} \tag{3.4}$$

where $l_{\mu}l^{\mu} = m_{\mu}m^{\mu} = n_{\mu}n^{\mu} = l_{\mu}m^{\mu} = n_{\mu}m^{\mu} = 0$ e $l_{\mu}n^{\mu} = -m_{\mu}\bar{m}^{\mu} = 1$ (in this case $\bar{x}$ is the complex conjugate of the general quantity x) for the spacetime (3.3) the null tetrad vectors are

$$\begin{aligned} l^{\mu} &= \delta_1^{\mu} \\ n^{\mu} &= \sqrt{\frac{F}{G}}\delta_0^{\mu} - \frac{1}{2}F\delta_1^{\mu} \\ m^{\mu} &= \frac{1}{2H}\left(\delta_2^{\mu} + \frac{i}{sin\theta}\delta_3^{\mu}\right) \end{aligned} \tag{3.5}$$

It is also convenient to use the tetrad notation introduced by Newman and Penrose for null tetrad vectors as $Z_a^{\mu} = (l^{\mu}, n^{\mu}, m^{\mu}, \bar{m}^{\mu}) \quad a = 1, 2, 3, 4$

- Extend the coordinates x^{ρ} to a new set of complex coordinates $\tilde{x}^{\rho}$

$$x^{\rho} \to \tilde{x}^{\rho} = x^{\rho} + iy^{\rho}\left(x^{\sigma}\right) \tag{3.6}$$

where $y^{\rho}\left(x^{\sigma}\right)$ are analytic functions of the real coordinates x^{σ} and simultaneously let the null tetrad vectors Z_a^{μ} undergo a transformation

$$Z_a^{\mu}\left(x^{\rho}\right) \to \tilde{Z}_a^{\mu}\left(\tilde{x}^{\rho}, \bar{\tilde{x}}^{\rho}\right) \tag{3.7}$$

It is required that the transformation recovers the old tetrad and metric when $\tilde{x}^{\rho} = \bar{\tilde{x}}^{\rho}$. The effect of this *tilde transformation* is to create a new metric whose components are (real) functions of complex variables such that

$$g_{\mu\nu} \to \tilde{g}_{\mu\nu} : \tilde{\mathbf{x}} \times \tilde{\mathbf{x}} \to \mathbb{R} \tag{3.8}$$

- The new metric is obtained from the particular choice of complexification chosen by Newman and Janis to generate the Kerr-Newman metric

$$x^{\rho} \to \tilde{x}^{\rho} = x^{\rho} + iacosx^2\left(\delta_0^{\rho} - \delta_1^{\rho}\right) \tag{3.9}$$

in this case we use the complex increment

$$\begin{aligned} r \to r' &= r + iacos\theta \\ u \to u' &= u - iacos\theta \end{aligned} \tag{3.10}$$

Obtaining the null tetrad vectors

$$\begin{aligned} l^\mu &= \delta_1^\mu \\ n^\mu &= \sqrt{\frac{F}{G}}\delta_0^\mu - \frac{1}{2}F\delta_1^\mu \\ m^\mu &= \frac{1}{2H}\left(iasin\theta\left(\delta_0^\mu - \delta_1^\mu\right) + \delta_2^\mu + \frac{i}{sin\theta}\delta_3^\mu\right) \end{aligned} \tag{3.11}$$

From these identities is possible to recover the general form of the transformed metric with the formula (3.4). We see that this procedure is the same as acting directly on the parameters of the metric written in Eddington-Finklenstein coordinates, so we have to write it only in the appropriate coordinates.
Hence we recall that in the simple case of $G = F$ and $H = r^2$ the metric in Eddington-Finklenstein coordinates can be written

$$ds^2 = G(r)du^2 + 2dudr - r^2d\Omega^2 \tag{3.12}$$

3.2 Application of Newman-Janis Algorithm

Taking our metric

$$ds^2 = \left(1 - \frac{2Mr}{r^2 + L_0^2}\right)dt^2 + \left(1 - \frac{2Mr}{r^2 + L_0^2}\right)^{-1}dr^2 + r^2d\Omega^2 \tag{3.13}$$

we write it in Eddington-Finkelstein coordinates as follows

$$ds^2 = G(r)du^2 + 2dudr - r^2d\Omega^2 \tag{3.14}$$

where

$$G(r) = 1 - \frac{2Mr}{r^2 + L_0^2} \tag{3.15}$$

Employing the above steps for applying NJA, it is introduced the complex increment

$$r \to r' = r + iacos\theta \tag{3.16}$$

where a is the rotation parameter. Then $G(r)$ is complexified as

$$G(r,\theta) = 1 - \frac{2Mr}{\Sigma + L_0^2} \tag{3.17}$$

Where $\Sigma = r^2 + a^2 cos^2\theta$.
For our porpouse we focus only on components g_{tt} and g_{rr}, both of them are essential to recover the trends of the event horizons and the photonsphere. It is possible to write the components in Boyer-Lindquist from Eddington-Finkelstein coordinates as

$$g_{tt} = G(r,\theta) \qquad\qquad g_{rr} = \frac{\Sigma(r,\theta)}{\Sigma(r,\theta)G(r,\theta) + a^2 sin^2\theta} \tag{3.18}$$

obtaining explicitly

$$\begin{aligned} g_{tt} &= 1 - \frac{2Mr}{\Sigma + L_0^2} \\ g_{rr} &= \frac{\Sigma^2 + \Sigma L_0^2}{\Sigma^2 + \Sigma\left(L_0^2 + a^2 sin^2\theta - 2Mr\right) + L_0^2 a^2 sin^2\theta} \end{aligned} \tag{3.19}$$

3.3 Event Horizons for the rotating case

Now we have all the tools for the study of EHs. For the sake of understanding it is reminded, in the following, the inner and outer horizons of Kerr metric

$$1/g_{rr} = 0 \to r_{int} = \frac{2M + \sqrt{2M - 4a^2}}{2} \qquad g_{tt} = 0 \to r_{out} = \frac{2M + \sqrt{2M - 4a^2 cos^2\theta}}{2}$$

To note that the above our components for $L_0 = 0$ recover exactly, as have to, the Kerr metric.
Returning to our metric, see how the parameters L_0, M and a are related from the domain of existence for $g_{tt} = 0$, that provide the condition

$$M^2 - L_0^2 - a^2 > 0 \tag{3.20}$$

This relation is verified for intervals

$$0 < L_0 < M,$$

$$-\sqrt{M^2 - L_0^2} < a < \sqrt{M^2 - L_0^2}$$

Choosing an average value of a as

$$a = \frac{1}{2}\sqrt{M^2 - L_0^2} \tag{3.21}$$

and respectively fixed the values for M and L_0, we can plot the results for $\theta = 0$ and $\theta = \pi/2$, in the adimensional and dimensional cases.
The horizons $1/g_{rr} = 0 \to r_{int}$ and $g_{tt} = 0 \to r_{out}$ assume the shape

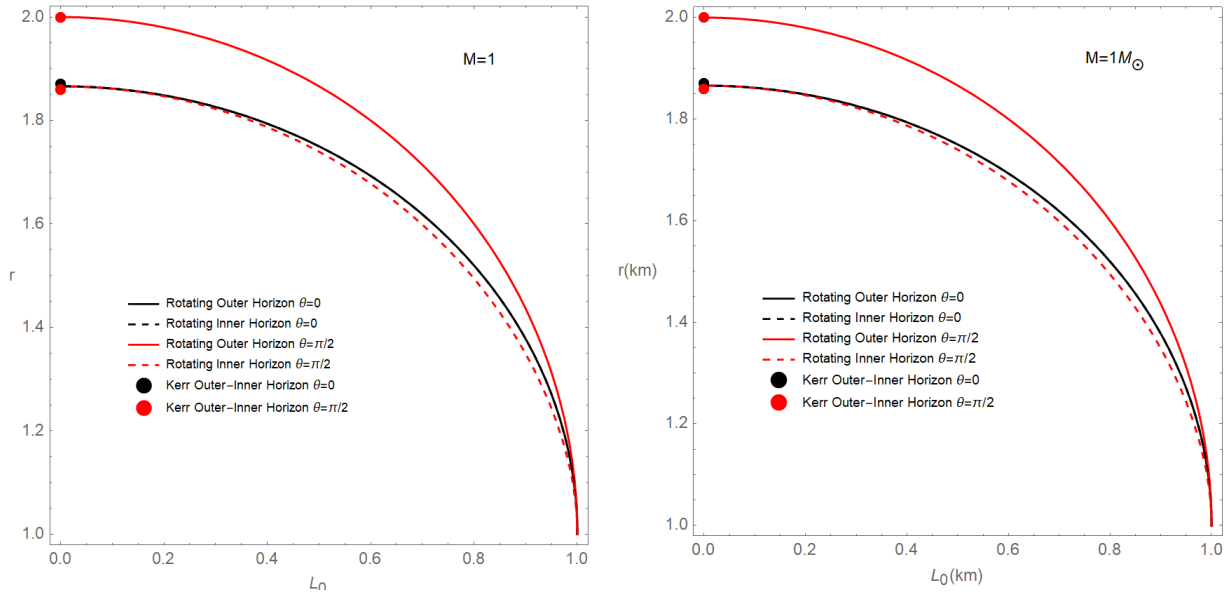

Figure 3.1: In black line is represented the outer horizon for $\theta = 0$, in black dotted line the inner horizon for $\theta = 0$, in red line the outer horizon for $\theta = \pi/2$, in red dotted line the inner horizon for $\theta = \pi/2$.

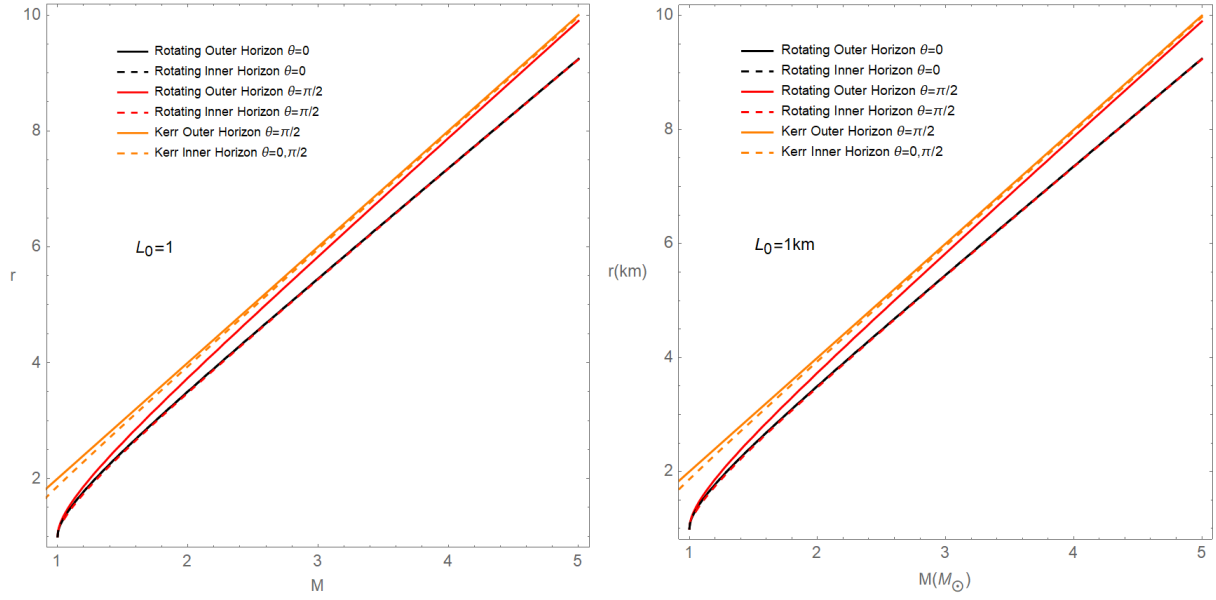

The colours distinguish the viewing angle. The horizons at $\theta = 0$ in black are overlapping not only for $L_0 = 0$, as have to from the results of General Relativity, but also for every value of L_0.
In red we have the horizons at $\theta = \pi/2$, in both cases we note a decreasing behavior in function of L_0.
Also in this case we can appreciate differences for only large value of L_0, in this unrealistic case we can appreciate differences $\sim km$ for $L_0 = 1km$.
In the graphs below, we can note the trend for L_0 fixed, and we can see as the ergosphere, the region between the outer and the inner horizon, is more large for bigger value of the mass.

3.4 Photon orbits for the rotating case

Last but not least, we approach the calculation of Photonsphere [22]. Restricting ourselves to the orbital, easier, case $\theta = \pi/2$, the metric assumes the form

$$ds^2 = g_{tt}dt^2 + 2g_{t\phi}dtd\phi + g_{\phi\phi}d\phi^2 + g_{rr}dr^2 \tag{3.22}$$

or explicitly

$$ds^2 = \left(1 - \frac{2Mr}{\Delta_{L_0}}\right)dt^2 + \left(\frac{4aMr}{\Delta_{L_0}}\right)dtd\phi - \left(\frac{r^2\Delta_{L_0}}{\Delta - 2Mr^3}\right)dr^2$$

$$- \left(\frac{\Delta + 2Mra^2}{\Delta_{L_0}}\right)d\phi^2 \tag{3.23}$$

Where $\Delta_{L_0} = L_0^2 + r^2$ and $\Delta = \Delta_{L_0}(a^2 + r^2) = \Delta_{L_0}\Delta_a$. This metric is independent of the coordinates t and ϕ and so we immediately have the two Killing vectors

$$\begin{aligned} \xi(t) &= (1, 0, 0, 0) \\ \xi(\phi) &= (0, 0, 0, 1) \end{aligned} \tag{3.24}$$

We choose the affine parameter λ along the trajectory so that $p^\mu = \dot{x}^\mu = dx^\mu/d\lambda$. Then the conserved quantities, the energy E and angular momentum L, are

$$\begin{aligned} E &= -\xi(t)_\mu p^\mu = -g_{tt}\dot{t} - g_{t\phi}\dot{\phi} \\ L &= \xi(\phi)_\mu p^\mu = g_{t\phi}\dot{t} + g_{\phi\phi}\dot{\phi} \end{aligned} \tag{3.25}$$

explicitly

$$E = -\left(1 - \frac{2Mr}{\Delta_{L_0}}\right)\dot{t} - \left(\frac{2aMr}{\Delta_{L_0}}\right)\dot{\phi}$$
$$L = \left(\frac{2aMr}{\Delta_{L_0}}\right)\dot{t} - \left(\frac{\Delta + 2Mra^2}{\Delta_{L_0}}\right)\dot{\phi} \tag{3.26}$$

while the normalization condition $p^2 = m^2$ takes the form

$$g_{tt}\dot{t}^2 + 2g_{t\phi}\dot{t}\dot{\phi} + g_{\phi\phi}\dot{\phi}^2 + g_{rr}\dot{r}^2 = m^2 \tag{3.27}$$

explicitly

$$\left(1 - \frac{2Mr}{\Delta_{L_0}}\right)\dot{t}^2 + \left(\frac{4aMr}{\Delta_{L_0}}\right)\dot{t}\dot{\phi} - \left(\frac{\Delta + 2Mra^2}{\Delta_{L_0}}\right)\dot{\phi}^2 - \\ + \left(\frac{r^2\Delta_{L_0}}{\Delta - 2Mr^3}\right)\dot{r}^2 = m^2 \tag{3.28}$$

Substituting (3.26) in (3.28) one obtains the variables $\dot{r}, \dot{t}$ and $\dot{\phi}$

$$\dot{r} = \pm\sqrt{\frac{E^2\left(\Delta + 2a^2Mr\right) + L^2\left(2Mr - \Delta_{L_0}\right) - m^2\left(2Mr^3 - \Delta\right) - 4aEMLr}{r^2\Delta_{L_0}}}$$

$$\dot{t} = \frac{-E\left(\Delta + 2a^2Mr\right) + 2aMLr}{\Delta - 2Mr^3}$$

$$\dot{\phi} = \frac{L\left(2Mr - \Delta_{L_0}\right) - 2aEMr}{\Delta - 2Mr^3} \tag{3.29}$$

It is convenient to use the proper time parameter $\tau = m\lambda$ and instead of the energy E and the angular momentum L, use the *specific energy* $E = E/m$ and the *specific angular momentum* $L = L/m$.
Equation (3.29) for $\dot{r}$ takes the form

$$\frac{dr}{d\tau} = \pm\sqrt{\frac{\mathcal{P}}{\Delta_r}} \tag{3.30}$$

The annulment of $\mathcal{P} = 0$ identify the turning points of the orbit. At these points we have $E = V_{\pm}$ and we can recognize the effective potential of the system.
In the vicinity of any turning point r_0, one can write a Taylor expansion of the function $\mathcal{P}$ as

$$\mathcal{P} = P_0 + P_1(r - r_0) + P_2(r - r_0)^2 + ... \tag{3.31}$$

A circular orbit is a special type of bounded motion when two of its turning points coincide with each other, and one has

$$P_0 = P_1 = 0 \tag{3.32}$$

Then, in the vicinity of the circular orbit, the radial equation takes the form

$$\frac{dr}{d\tau} = \pm\sqrt{\frac{P_2}{\Delta_r}}(r - r_0) \tag{3.33}$$

From (3.32) is possible to establish a relation between three quantities r_{circ}, E_{circ} and L_{circ} which characterize the circular motion. In particular we focus on E_{circ} to find the photonsphere.
Indeed it is recovered from the value of r that send it to infinity.
Then, we compare some values of L_0 with the case of Kerr ($L_0 = 0$). In the following plot we see how the inner horizon varies as L_0 varies.

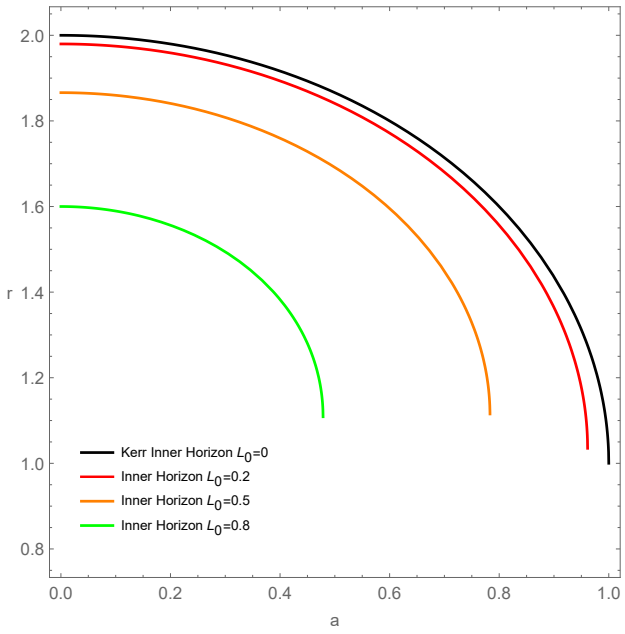

Figure 3.2: Note the change of the inner horizon as change of L_0, the various colour indicates the various L_0, the black line indicates the Kerr case

While the photonsphere assumes the form

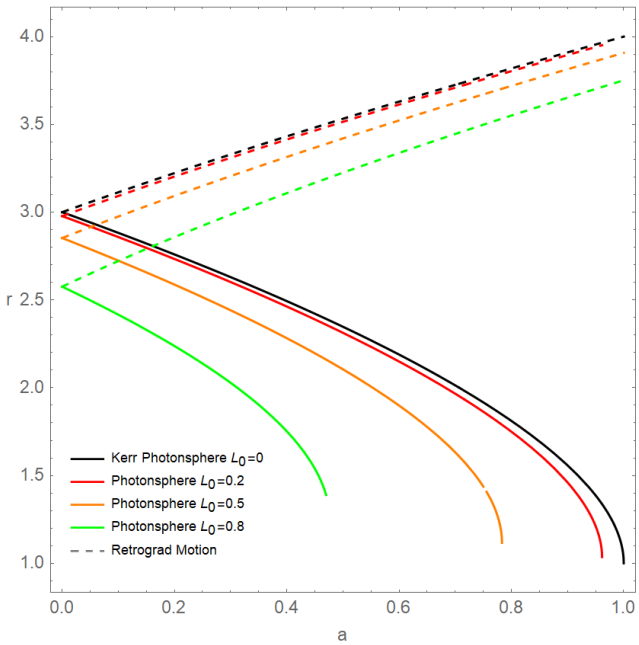

Figure 3.3: With the same above indications on the colour, we distinguish also the direct motion and the retrograd motion with the dotted lines

Last, we consider the photonsphere and the inner horizon together

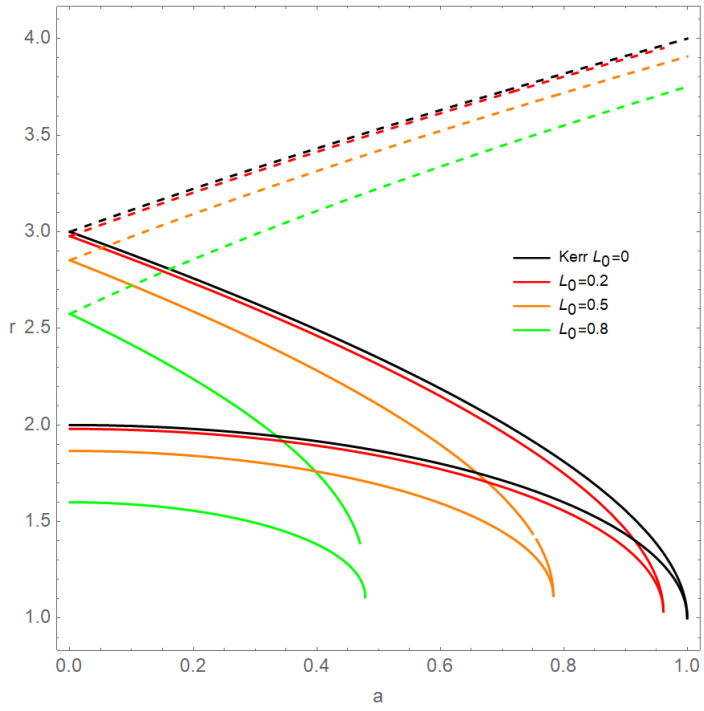

Figure 3.4: With the same above indications on the colour, we can control the consistency of results

Furthermore we can also note that for $a = 0$, when we return to a static case, there is no difference between prograde and retrograd motion as have to, and this happens for every value of L_0.
In this adimensional case, the dimension is given by the unit of measure of L_0, if $L_0 \sim km$ so $r \sim km$, if $L_0 \sim L_P$ so $r \sim L_P$ and so on.

Chapter 4

Shadows

4.1 The Black Hole's shadow

A century has passed from the calculation that in 1919 allowed the verification of General Relativity from the deviation of light due to the solar eclipse [49], to the demonstration of the existence of the shadow of a black hole. It was been a very success for the theory, that a mighty evidence like this, it is now possible to see for our instrument (Event Horizon Telescope's collaboration [2]-[7]). Not only for the public, namely for the fact that it gives a visual appearance of how a black hole looks like, but also for the possibility to discriminate the various theories with their parameters, to discriminate the various types of black holes or to discriminate objects called black holes mimickers or black holes impostors, which are very massive objects but are not black holes at all. Therefore, the importance of the shadows are increasing in this epoch, as the instrument to evidence them are increasing.
For this reason, we approach the study of the shadow in static and rotating case of our metric as the parameter L_0 changes.
Before focusing our attention on the calculation, it is convenient to recall the definition of shadow and of the background in which we study it. There is such confusion around the definition of a shadow. For the inexpert public, it is regarded as the image of the darkness spot created by the event horizon.
In reality, it is true that the event horizon corresponds to the maximum distance where the light can escape, but the shadow represents the boundary between the light geodesics in stable orbits and the light geodesics in unstable orbits, where the light geodesics present instability on the radius component, so it contains both the photon orbit and the event horizon.
In particular, as evidenced from the work of J. L. Synge [50], where he studies the case of a Schwarzschild black hole and the word shadow did not exist yet, the

angular size under which an observer, at a large distance, would see the black hole is approximately 2.5 times more bigger than of the angular size of the effective horizon. We can recall also the work of Zeldovich and Novikov [51], and the work of V. Perlick and O. Tsupko [52] which in a very similar way calculate this quantity. The angular size of a black hole can be understood from the following figure.

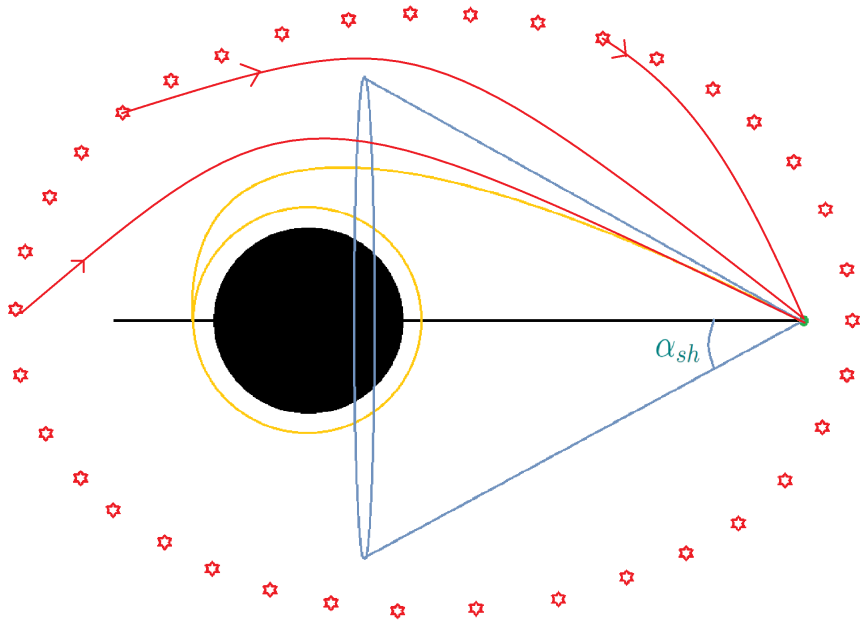

Figure 4.1: It is represented the shadow of a static black hole and its photonsphere, the green ball represents the observer.

For the background in which the shadow is studied, it is considered a uniform distribution of light sources beneath the black hole.
For simplicity it is not considered any light sources between the black hole and the observer. In this idealization, the observer issues the light rays in the past, some reach the light source, some not.
The limit of these two types of light defines the shape of the shadow.
It is clear that this idealization is far from the reality, where we have light sources everywhere between the black hole and the observer and where some light rays are deflected or absorbed. However it is a very powerful instrument to have an idea of the behavior of a black hole.
Furthermore, there is a difference between the static and the rotating case of the shadow.
The first case is the most easy, because the attention is focused more on the angu-

lar size of the shadow than on the shadow itself, and we recall the principal work already cited of J. L. Synge [50] followed by V. Perlick and O. Tsupko [52] and A. Grenzebach, V. Perlick, and C. Lammerzahl [53].
The second case, on the contrary, is more complicated due to rotation that flattens the shadow on one side, and by the fact that we have a photon region rather than a photon sphere due to retrograde and prograde motion of the light geodesics. In this case we can recall besides the last two work also the principal works of J. M. Bardeen [54] and S. Chandrasekhar [55].

4.2 Shadow in static case

Using the background discussed before, we follow the calculation from the work of V. Perlick and O. Tsupko [52] based on the work of J. L. Synge [50].
It is considered the more general case of spherically symmetric static metric

$$g_{\mu\nu}dx^{\mu}dx^{\nu} = -A(r)dt^2 + B(r)dr^2 + D(r)\left(d\theta^2 + sin^2\theta d\varphi^2\right) \tag{4.1}$$

Here we consider $c = 1$. For this metric we can write the Lagrangian

$$\mathcal{L}(x,\dot{x}) = \frac{1}{2}\left(-A(r)\dot{t}^2 + B(r)\dot{r}^2 + D(r)(\dot{\theta}^2 + sin^2\theta\dot{\varphi}^2)\right) \tag{4.2}$$

Thanks to the symmetry we can consider the geodesics in the equatorial plane placing $\theta = \pi/2$ and $sin\theta = 1$.
From the Eulero Lagrange equation

$$\frac{d}{d\lambda}\left(\frac{\partial\mathcal{L}}{\partial\dot{x}^{\mu}}\right) - \frac{\partial\mathcal{L}}{\partial x^{\mu}} = 0 \tag{4.3}$$

we can obtain the components for t and φ that provide us the constants of motion

$$E = A(r)\dot{t}^2, \qquad L = D(r)\dot{\varphi} \tag{4.4}$$

Substituting these constants in the first integral of geodetic equation $g_{\mu\nu}\dot{x}^{\mu}\dot{x}^{\nu} = 0$, i.e.

$$-A(r)\dot{t}^2 + B(r)\dot{r}^2 + D(r)\dot{\varphi}^2 = 0 \tag{4.5}$$

we can have the orbits of light geodesics

$$\left(\frac{dr}{d\varphi}\right)^2 = \frac{D(r)}{B(r)}\left(\frac{D(r)}{A(r)}\frac{E^2}{L^2} - 1\right) \tag{4.6}$$

The ratio of the two constants of motion L/E represents the so called impact parameter b, it can be defined as the limit from the center of a black hole to the border between stable and unstable photon orbit.
In the point where $dr/d\varphi = 0$, we have a turning point or the minimum distance for a light ray, we called this turning point R. Hence, we can identify the following relation

$$\frac{1}{b^2} = \frac{E^2}{L^2} = \frac{A(R)}{D(R)} \tag{4.7}$$

Considering also the function $h^2(r) = D(r)/A(r)$, inserting all these relations in (4.6), we obtain

$$\left(\frac{dr}{d\varphi}\right)^2 = \frac{D(r)}{B(r)}\left(\frac{h^2(r)}{h^2(R)} - 1\right) \tag{4.8}$$

In the idealization of the computation, it is considered that an observer issues a light ray in the past towards a black hole, so the angular size α between this light ray and the radial direction is given by

$$sin^2\alpha = \frac{h^2(R)}{h(r_0)} \tag{4.9}$$

Where r_0 is the distance from the observer. In the limit, in which the light ray approaches the unstable orbit $R \to r_{ph}$, is obtained the angular size of the shadow

$$sin^2\alpha_{sh} = \frac{h^2(r_{ph})}{h(r_0)} \tag{4.10}$$

The photon sphere for the static case is obtained in Chapter 1

$$L_0^4 + r_{ph}^3(-3M + r_{ph}) + L_0^2 r_{ph}(-M + 2r_{ph}) = 0 \tag{4.11}$$

In our metric $A(r) = 1 - 2Mr/r^2 + L_0^2$ and $D(r) = r^2$, then $h^2(r)$ will be

$$h^2(r) = \frac{r^2}{1 - \frac{2Mr}{r^2+L_0^2}} \tag{4.12}$$

For an observer at large distance from the black hole $r_0 >> 3M$, the formula, for the angular size, is simplified as

$$\alpha_{sh} = \frac{h(r_{ph})}{r_0} \tag{4.13}$$

Hence, in the following, we show some results for some values of L_0

$M = 1$	$L_0 = 0$	$L_0 = 0.2$	$L_0 = 0.5$	$L_0 = 0.8$
$r_0\alpha_{sh}$	$3\sqrt{3}$ (5.196)	5.172	5.044	4.767

This shows as the angular size decreases when L_0 increases, obviously for $L_0 = 0$ we recover the Schwarzschild case as it has to.

4.3 Shadow in rotating case

We are now ready to introduce the shadow for the more complicate rotating case [52]. The complicate nature of this situation is due to the rotating parameter that for our purpose depends on M and L_0, i.e.

$$a \leq \sqrt{M^2 - L_0^2} \tag{4.14}$$

deducible from the existence condition of the event horizon.
Furthermore there is the problem of the photon orbit, not more made of circular lightlike geodesics but made of spherical lightlike geodesics called photon sphere or photon shell [56].
The difference is the existence of a prograde and retrograde motion that changes as a changes, shaping the shadow in a peculiar way.
Anyway the aim is to deduce the shadow from the limit in wich the lightlike geodesics approach the orbit. To this purpose we rely on four constants of motion:

- the first integral, used also in the static case, of the geodetic equation $g_{\mu\nu}\dot{x}^\mu\dot{x}^\nu = 0$,
- the z-component of angular momentum and the energy derived from the symmetries of the system for t and φ,
- the Carter constant K derived from the separability of the Hamilton-Jacobi equation for geodesics [57]

To begin with, the setting of our idealization is fundamental.
We consider, like before, a light ray issued from an observer distant r_0 from the black hole to an angle ϑ_0 in Boyer-Lindquist coordinates [53]. In the observer's reference system we introduce a tetrad e_μ

$$\begin{aligned} e_0 &= \left.\frac{(r^2+a^2)\,\partial t + a\partial\varphi}{\sqrt{\Sigma\Delta_r}}\right|_{r_0,\vartheta_0} \\ e_1 &= \left.\sqrt{\frac{1}{\Sigma}}\partial\vartheta\right|_{r_0,\vartheta_0} \\ e_2 &= \left.-\frac{(\partial\varphi + asin^2\vartheta\partial t)}{\sqrt{\Sigma}sin\vartheta}\right|_{r_0,\vartheta_0} \\ e_3 &= \left.-\sqrt{\frac{\Delta_r}{\Sigma}}\partial r\right|_{r_0,\vartheta_0} \end{aligned} \tag{4.15}$$

where we have introduced the quantities

$$\Sigma = r^2 + a^2 cos^2\vartheta$$

$$\Delta_r = g_{rr}^{-1}\Sigma = \Sigma - \frac{2Mr\Sigma}{(\Sigma + L_0^2)} + a^2 sin^2\vartheta$$

This tetrad has the property that the surfaces $e_0 + e_3$ and $e_0 - e_3$ are tangetial respectively to ingoing and outgoing lightlike geodesics issued in the past, it is useful to look the Figure 4.3 of the work [53].

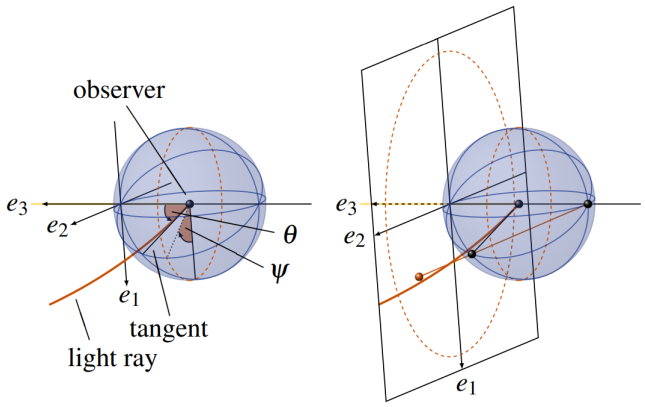

Figure 4.2: It is shown the tetrad respect to the observer and the stereographic projection from celestial sphere of point (θ, ψ). See figure 8 in work of A. Grenzebach, V. Perlick, and C. Lammerzahl [53]

The tangent vector of the light ray $\lambda(s)$ in the observer's reference system can be write

$$\dot{\lambda} = -e_0 + sin\theta cos\psi e_1 + sin\theta sin\psi e_2 + cos\theta e_3 \tag{4.16}$$

Equaling the coefficients of $\partial\varphi$ and ∂r in (4.16) and (4.15) and substituting the solutions for $\dot{\varphi}$ and $\dot{r}$ from the Eulero-Lagrange in there, we obtain the final outcomes

$$\begin{aligned} sin\psi &= \frac{L_E(r_{ph})}{\sqrt{K_E(r_{ph})}} \\ sin\theta &= \frac{\sqrt{\Delta_r(r_0)K_E(r_{ph})}}{r_0 - aL_E} \end{aligned} \tag{4.17}$$

Some constants are introduced such as

$$aL_E = \frac{aL_z}{E} = r^2 - \frac{4r\Delta_r}{\Delta_r'} \qquad K_E = \frac{K}{E^2} = \frac{16r^2\Delta_r}{(\Delta_r')^2} \tag{4.18}$$

Here, r_{ph} can be seen as the spherical light orbit which a light ray with azimutal angle ψ towards in.
The value (θ, ψ) represents a point in the celestial sphere, as it is shown in Figure 4.3. At fixed θ, changing ψ from $[-\pi/2, \pi/2]$ we obtain the lower shape of the shadow, and for symmetry we obtain the upper one.

It is recovered also the last static case if we consider the case for $a = 0$ and $r_{ph} = 3M$ where in this case θ represents our α_{sh}.
After all this mathematics digression, we are able to plot the shadows using the stereographic projection of the celestial sphere on a plane tangent to $\theta = 0$ thanks to the transformations (see formula [53]-[54] in [53])

$$x(r_{ph}) = -2tan\left(\frac{\theta_{r_{ph}}}{2}\right) sin\left(\psi(r_{ph})\right)$$
$$y(r_{ph}) = -2tan\left(\frac{\theta_{r_{ph}}}{2}\right) cos\left(\psi(r_{ph})\right) \tag{4.19}$$

In the following, we plot the shadows as L_0 changes.

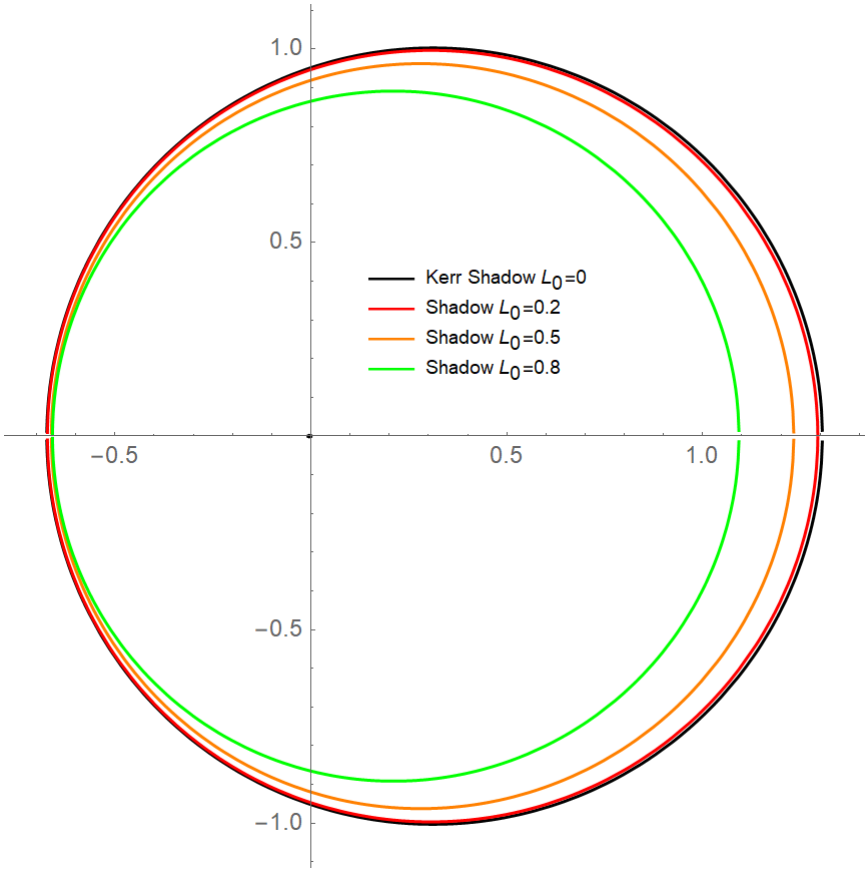

Figure 4.3: Color lines represent the various L_0 respectively red for $L_0 = 0.2$, orange for $L_0 = 0.5$, green for $L_0 = 0.8$, in black is shown the Kerr metric for $L_0 = 0$, from a distance $r_0 = 5M$ ($a = 50\%, M = 1, \theta = \pi/2$)

This plot is made with a rotation parameter $a = 50\%$ of the maximum allowed

value from the formula (4.14), and as we expect, for $L_0 = 0$ the Kerr metric is recovered. There is a consistent similitude with the Kerr case, with a contraction of the shadow when L_0 grows as we expected from the study of photonsphere in Chapter 3 Figure 3.4.
If we want to study how the plots look like, for $a = 80\%$ and $a = 99\%$ of the maximum allowed value, see Figure 4.4 - 4.5 below, where it is shown a pathological behavior near the flattened side, more accentuated as a grows despite the major axis of the shadow is consistent with Kerr.
Hence it can be considered as an observable deviation from the canonical solutions of Kerr.
Furthermore, we can note also the consistency with the static case where the angular size decreases when L_0 grows (see section 4.1), in this case the same occurs with a decreasing of the shadow.

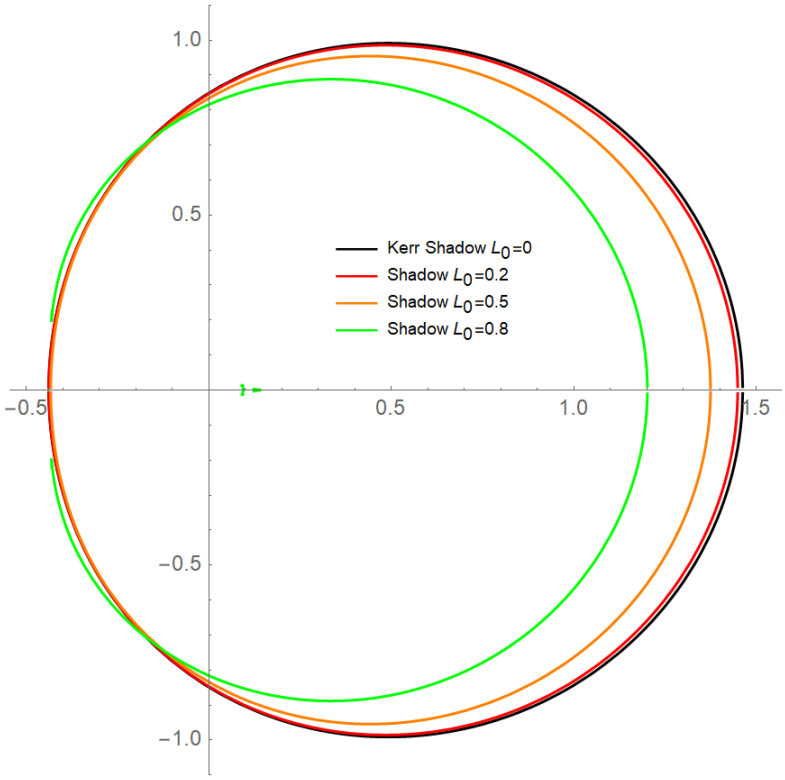

Figure 4.4: Color lines represent the various L_0 , in black is shown the Kerr metric, from a distance $r_0 = 5M$ ($a = 80\%, M = 1, \theta = \pi/2$)

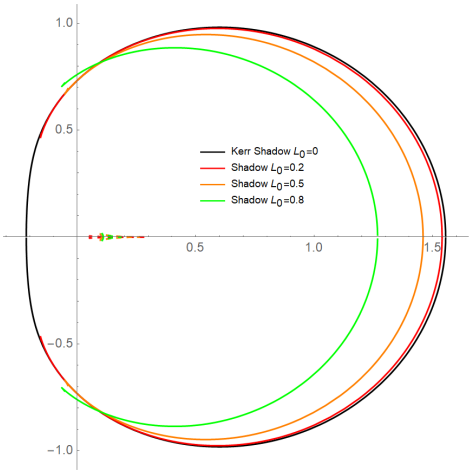

Figure 4.5: Color lines represent the various L_0, in black is shown the Kerr metric, from a distance $r_0 = 5M$ ($a = 99\%, M = 1$,$\theta = \pi/2$)

Let us concentrate to the first case of closed shadows. We can study the deviation with respect to General Relativity and so to the Kerr case for $L_0 = 0$, studying three parameters that distinguish the shadows [58]. The major axis $\Delta\beta$, the minor axis $\Delta\alpha$ and the axis ratio $\delta = \Delta\beta/\Delta\alpha$ which we can visualize in the following image

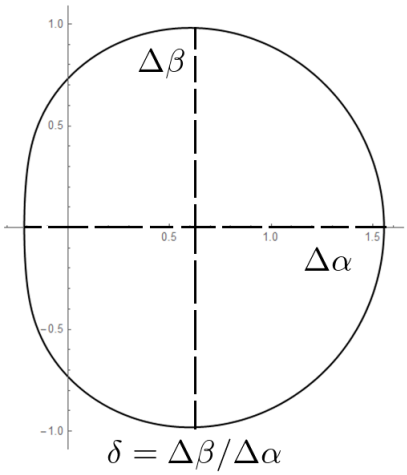

Figure 4.6: There are represented the delta axes of a rotating shadow

From these quantities is possible to understand if EHT can estimate these differences. The mass of M87 is $6,6 * 10^9 M_\odot = 6,6 * 10^{47} M_P$, also if for absurd, we

$M=1$, $a=0.5$	Kerr case	$L_0=0.2$	$L_0=0.5$	$L_0=0.8$
$\Delta\beta$	2.007	1.995 (-0.6%)	1.931 (-3.9%)	1.783 (-12.6%)
$\Delta\alpha$	1.978	1.966 (-0.6%)	1.898 (-4.2%)	1.752 (-12.9%)
δ	1.0146	1.0147 (+ 0.01%)	1.0173 (+0.26%)	1.0171 (+0.24%)

Table 4.1: In the table is represented respectively the major axis, the minor axis and the axis ratio versus L_0. In parenthesis is indicated the rate difference with General Relativity

consider an $L_0 = 10^{47} L_P = 10^{12} m$, we are in the range where $L_0 \sim 0.2$ of the maximum allowed for this mass, so we would appreciate a deviation of the $0,6\%$ in the major axis.
We recall that the ring diameter observed for M87 is $\sim 42\mu as$.
The difference of 0.6% for $L_0 = 0.2$ is saying that we should appreciate the difference for an angular resolution of $\sim 0.25\mu as$. If now it is possible appreciate $\sim 25\mu as$ with the actual technology, we must have a 100 times better angular resolution and this is possible for an observable wavelength of $\lambda \sim 13\mu m$ or a diameter of our virtual telescope D 100 times bigger (Recall that the formula of the angular resolution is $\sim \lambda/D$).
But we expect L_0 to be roughly the Planck length, 47 orders of magnitude shorter than the one in use, so even with the most generous approach, we can say that current technology is not enough, moreover we would have a precise parameter of rotation.
Now we approach the study of opened shadows. If the parameter rotation a and the ratio between the fundamental length L_0 and the mass M increase, we can observe this strange behavior of the shadows that predict an intriguing possibility, the naked singularities.
In this case, the inner horizon fades out and it makes sense considering the extension for $r_{ph} < 0$, from which it emerges a dark spot represented by an area inaccessible to us because the light runs from the other side to $r = -\infty$. In figure is represented by a dashed area in the shadows.
These shadows have point of contact with the work [59] where in that case is considered a braneworld black hole. The shadows are influenced by the tidal charge Q due to the action of the gravitational force in a background of five dimensions. So this parameter can have some affinity with L_0. The considerations are taken from the study of the naked singularity in highly spinning Kerr metric of the work [60].

We can consider also a range of mass candidates to establish a possibility to observe this astrophysical phenomenon.
If the rotation parameter $a = 80\%$, we can observe a naked singularity from $L_0 = 0.8$ of the maximum allowed.
If $1L_P < L_0 < 10^{20}L_P$, we can observe them in a range of $1,2M_P < M < 1,2 \times 10^{20}M_P = 1.2 \times 10^{-18}M_\odot$.
While if the rotation parameter $a = 99\%$, we can observe a naked singularity from $L_0 = 0.2$ of the maximum allowed.
If $1L_P < L_0 < 10^{20}L_P$, we can observe them in a range of $5M_P < M < 5 \times 10^{20}M_P = 5 \times 10^{-18}M_\odot$.

Conclusions

We saw at the beginning the static case of our metric. Thanks to the results of these first considerations, it was possible to establish consistency with this metric, containing an arbitrary fundamental length L_0.
Indeed for parameter's value tending to zero we have recovered the classical case of the General Relativity for event horizons and photon sphere, as expected. Furthermore, we can see the tendency of the timelike circular orbits to the variation of the angular momentum L^2.
Beginning from the static metric and using the Newman-Janis algorithm, we were able to obtain a rotating metric for a more realistic case to be tested.
In this background it has been possible to observe contact points with the Kerr solution. It was interesting to note that the inner and the outer horizons are the same not only for $L_0 = 0$ and $\theta = 0$ as they expected, but this result is true also for every parameter of L_0.
Furthermore, for L_0 fixed, we can see that the ergosphere increases as M increases.
Meanwhile in general, for other possible values of L_0 and θ , both for event horizons and for photon orbits there is a decreasing trend when the mass M approaches the order of magnitude of L_0.
In the last Chapter we have approached the study of the shadows for the rotating case. These results are the most intriguing ones.
We plotted the various shadows when both L_0 and a, the rotation parameter, change. For a mean value of a, the shadows decrease their shape as L_0 decreases, and for high rotations a we have opened shadows.
This behavior unlikely provides a possibility to establish the value of the fundamental length from some future observations, depending heavily by the orders of magnitude of L_0.
Now we present possible ways to detect it:

- Increasing the sensibility of our instruments (as surely EHT collaboration will do), this deviation will be more consistent for smaller and closer black holes.

- By creating mini black holes in laboratory with the advancements in the increasing of the energy of the particles accelerators as LHC [61].
- Searching for astrophysical objects related to the naked singularities as black holes with a darker area in the shadow [60].
- Considering that this very small black holes highly rotating have the effect to curve the light providing an explanation to the dark matter actually composed of mini black holes.
  In this case it would be possible to estimate L_0 substituting a density of dark matter with mini black holes, and calculating the deflection of the light, and so matching the value of L_0.

Bibliography

[1] Gia Dvali and Cesar Gomez. "Self-Completeness of Einstein Gravity". In: *arXiv e-prints*, arXiv:1005.3497 (May 2010), arXiv:1005.3497. arXiv: 1005.3497 [hep-th].

[2] Event Horizon Telescope Collaboration et al. "First M87 Event Horizon Telescope Results. I. The Shadow of the Supermassive Black Hole". In: 875.1, L1 (Apr. 2019), p. L1. DOI: 10.3847/2041-8213/ab0ec7. arXiv: 1906.11238 [astro-ph.GA].

[3] Event Horizon Telescope Collaboration et al. "First M87 Event Horizon Telescope Results. I. The Shadow of the Supermassive Black Hole". In: 875.1, L1 (Apr. 2019), p. L1. DOI: 10.3847/2041-8213/ab0ec7. arXiv: 1906.11238 [astro-ph.GA].

[4] Event Horizon Telescope Collaboration et al. "First M87 Event Horizon Telescope Results. III. Data Processing and Calibration". In: 875.1, L3 (Apr. 2019), p. L3. DOI: 10.3847/2041-8213/ab0c57. arXiv: 1906.11240 [astro-ph.GA].

[5] Event Horizon Telescope Collaboration et al. "First M87 Event Horizon Telescope Results. IV. Imaging the Central Supermassive Black Hole". In: 875.1, L4 (Apr. 2019), p. L4. DOI: 10.3847/2041-8213/ab0e85. arXiv: 1906.11241 [astro-ph.GA].

[6] Event Horizon Telescope Collaboration et al. "First M87 Event Horizon Telescope Results. V. Physical Origin of the Asymmetric Ring". In: 875.1, L5 (Apr. 2019), p. L5. DOI: 10.3847/2041-8213/ab0f43. arXiv: 1906.11242 [astro-ph.GA].

[7] Event Horizon Telescope Collaboration et al. "First M87 Event Horizon Telescope Results. VI. The Shadow and Mass of the Central Black Hole". In: 875.1, L6 (Apr. 2019), p. L6. DOI: 10.3847/2041-8213/ab1141. arXiv: 1906.11243 [astro-ph.GA].

[8] Dimitrios Psaltis et al. “Gravitational Test beyond the First Post-Newtonian Order with the Shadow of the M87 Black Hole”. In: 125.14, 141104 (Oct. 2020), p. 141104. DOI: 10.1103/PhysRevLett.125.141104. arXiv: 2010.01055 [gr-qc].

[9] B. P. Abbott et al. “Tests of General Relativity with GW150914”. In: 116.22, 221101 (June 2016), p. 221101. DOI: 10.1103/PhysRevLett.116.221101. arXiv: 1602.03841 [gr-qc].

[10] Piero Nicolini and Euro Spallucci. “Holographic screens in ultraviolet self-complete quantum gravity”. In: *arXiv e-prints*, arXiv:1210.0015 (Sept. 2012), arXiv:1210.0015. arXiv: 1210.0015 [hep-th].

[11] Martin Sprenger, Piero Nicolini, and Marcus Bleicher. “Quantum Gravity Signals in Neutrino Oscillations”. In: *International Journal of Modern Physics E* 20 (Jan. 2011), pp. 1–6. DOI: 10.1142/S0218301311040517. arXiv: 1111.2341 [hep-ph].

[12] E. T. Newman and A. I. Janis. “Note on the Kerr Spinning-Particle Metric”. In: *Journal of Mathematical Physics* 6.6 (June 1965), pp. 915–917. DOI: 10.1063/1.1704350.

[13] Giampiero Esposito. “An introduction to quantum gravity”. In: *arXiv e-prints*, arXiv:1108.3269 (Aug. 2011), arXiv:1108.3269. arXiv: 1108.3269 [hep-th].

[14] Fabian Wagner. “Relativistic extended uncertainty principle from space-time curvature”. In: 105.2, 025005 (Jan. 2022), p. 025005. DOI: 10.1103/PhysRevD.105.025005. arXiv: 2111.15583 [gr-qc].

[15] G. Veneziano. “Construction of a crossing-simmetric, Regge-behaved amplitude for linearly rising trajectories”. In: *Nuovo Cimento A Serie* 57.1 (Sept. 1968), pp. 190–197. DOI: 10.1007/BF02824451.

[16] Leonard Susskind. “Structure of Hadrons Implied by Duality”. In: 1.4 (Feb. 1970), pp. 1182–1186. DOI: 10.1103/PhysRevD.1.1182.

[17] Leonard Susskind. “Harmonic-Oscillator Analogy for the Veneziano Model”. In: 23.10 (Sept. 1969), pp. 545–547. DOI: 10.1103/PhysRevLett.23.545.

[18] L. Susskind. “Dual-symmetric theory of hadrons.—I”. In: *Nuovo Cimento A Serie* 69.3 (Oct. 1970), pp. 457–496. DOI: 10.1007/BF02726485.

[19] Y. Nambu. “Quark model and the factorization of the Veneziano amplitude”. In: *Symmetries and Quark Models*. Ed. by Ramesh Chand. Jan. 1970, p. 269.

[20] Lars Brink, John H. Schwarz, and J. Scherk. “Supersymmetric Yang-Mills theories”. In: *Nuclear Physics B* 121.1 (Mar. 1977), pp. 77–92. DOI: 10.1016/0550-3213(77)90328-5.

[21] J. Scherk and John H. Schwarz. “How to get masses from extra dimensions”. In: *Nuclear Physics B* 153 (June 1979), pp. 61–88. DOI: 10.1016/0550-3213(79)90592-3.

[22] A. Zelnikov V. Frolov. *Introduction to Black Hole Physics*. Oxford University Press, 2011. ISBN: 9780199692293.

[23] K. Schwarzschild. “On the Gravitational Field of a Mass Point According to Einstein’s Theory”. In: *Abh. Konigl. Preuss. Akad. Wissenschaften Jahre 1906,92, Berlin,1907* 1916 (Jan. 1916), pp. 189–196.

[24] A. S. Eddington. “A Comparison of Whitehead’s and Einstein’s Formulæ”. In: 113.2832 (Feb. 1924), p. 192. DOI: 10.1038/113192a0.

[25] Roy P. Kerr. “Gravitational Field of a Spinning Mass as an Example of Algebraically Special Metrics”. In: 11.5 (Sept. 1963), pp. 237–238. DOI: 10.1103/PhysRevLett.11.237.

[26] Ezra Newman and Tim Adamo. “Kerr-Newman metric”. In: *Scholarpedia* 9.10 (Jan. 2014), p. 31791. DOI: 10.4249/scholarpedia.31791. arXiv: 1410.6626 [gr-qc].

[27] S. W. Hawking. “Particle creation by black holes”. In: *Communications in Mathematical Physics* 43.3 (Aug. 1975), pp. 199–220. DOI: 10.1007/BF02345020.

[28] Ajit Kumar Mehta et al. “Observing Intermediate-mass Black Holes and the Upper Stellar-mass gap with LIGO and Virgo”. In: *Astrophys. J.* 924.1 (2022), p. 39. DOI: 10.3847/1538-4357/ac3130. arXiv: 2105.06366 [gr-qc].

[29] S. Bowyer et al. “Cosmic X-ray Sources”. In: *Science* 147.3656 (Jan. 1965), pp. 394–398. DOI: 10.1126/science.147.3656.394.

[30] Jerome A. Orosz et al. “The Mass of the Black Hole in Cygnus X-1”. In: 742.2, 84 (Dec. 2011), p. 84. DOI: 10.1088/0004-637X/742/2/84. arXiv: 1106.3689 [astro-ph.HE].

[31] Guillaume Mahler et al. “Gravitational lensing effects of supermassive black holes in cluster environments”. In: *arXiv e-prints*, arXiv:2201.10900 (Jan. 2022), arXiv:2201.10900. arXiv: 2201.10900 [astro-ph.CO].

[32] B. P. Abbott et al. “Observation of Gravitational Waves from a Binary Black Hole Merger”. In: 116.6, 061102 (Feb. 2016), p. 061102. DOI: 10.1103/PhysRevLett.116.061102. arXiv: 1602.03837 [gr-qc].

[33] Ligo Collaboration. *What is LIGO*. URL: https://www.ligo.caltech.edu/page/what-is-ligo.

[34] Virgo Collaboration. *What is Virgo*. URL: https://www.virgo-gw.eu/#about.

[35] Leonard Susskind. "The world as a hologram". In: *Journal of Mathematical Physics* 36.11 (Nov. 1995), pp. 6377–6396. DOI: 10.1063/1.531249. arXiv: hep-th/9409089 [hep-th].

[36] Jacob D. Bekenstein. "Entropy bounds and black hole remnants". In: 49.4 (Feb. 1994), pp. 1912–1921. DOI: 10.1103/PhysRevD.49.1912. arXiv: gr-qc/9307035 [gr-qc].

[37] C. R. Stephens, G. 't Hooft, and B. F. Whiting. "Black hole evaporation without information loss". In: *Classical and Quantum Gravity* 11.3 (Mar. 1994), pp. 621–647. DOI: 10.1088/0264-9381/11/3/014. arXiv: gr-qc/9310006 [gr-qc].

[38] Thomas Berry, Alex Simpson, and Matt Visser. "Photon Spheres, ISCOs, and OSCOs: Astrophysical Observables for Regular Black Holes with Asymptotically Minkowski Cores". In: *Universe* 7.1 (Dec. 2020), p. 2. DOI: 10.3390/universe7010002. arXiv: 2008.13308 [gr-qc].

[39] LIGO Collaboration. *Detection Papers*. URL: https://www.ligo.caltech.edu/page/detection-companion-papers.

[40] Enrico Barausse et al. "Prospects for fundamental physics with LISA". In: *General Relativity and Gravitation* 52.8, 81 (Aug. 2020), p. 81. DOI: 10.1007/s10714-020-02691-1. arXiv: 2001.09793 [gr-qc].

[41] D. Angal-Kalinin et al. "Machine Layout and Performance". In: *arXiv e-prints*, arXiv:1705.09447 (May 2017), arXiv:1705.09447. arXiv: 1705.09447 [physics.acc-ph].

[42] E. T. Newman and A. I. Janis. "Note on the Kerr Spinning-Particle Metric". In: *Journal of Mathematical Physics* 6.6 (June 1965), pp. 915–917. DOI: 10.1063/1.1704350.

[43] S. P. Drake and R. Turolla. "The application of the Newman - Janis algorithm in obtaining interior solutions of the Kerr metric". In: *Classical and Quantum Gravity* 14.7 (July 1997), pp. 1883–1897. DOI: 10.1088/0264-9381/14/7/021. arXiv: gr-qc/9703084 [gr-qc].

[44] Stefano Viaggiu. “Interior Kerr Solutions with the Newman-Janis Algorithm Starting with Static Physically Reasonable Space-Times”. In: *International Journal of Modern Physics D* 15.9 (Jan. 2006), pp. 1441–1453. DOI: 10.1142/S0218271806009169. arXiv: gr-qc/0603036 [gr-qc].

[45] P. S. Florides. “A rotating sphere as a possible source of the Kerr metric”. In: *Nuovo Cimento B Serie* 13.1 (Jan. 1973), pp. 1–18. DOI: 10.1007/BF02726690.

[46] Rosangela Canonico, Luca Parisi, and Gaetano Vilasi. “The Newman Janis Algorithm: A Review of Some Results”. In: *Proc. Geom. Int. Quant.* 12 (2011). Ed. by Ivailo Mladenov, Gaetano Andrei Vilasi, and Akira Yoshiokoa, pp. 159–169. DOI: 10.7546/giq-12-2011-159-169.

[47] S. P. Drake and Peter Szekeres. “Uniqueness of the NewmanâJanis Algorithm in Generating the KerrâNewman Metric”. In: *General Relativity and Gravitation* 32.3 (2000), 445â457. ISSN: 1572-9532. DOI: 10.1023/a:1001920232180. URL: http://dx.doi.org/10.1023/A:1001920232180.

[48] Leonardo Modesto and Piero Nicolini. “Charged rotating noncommutative black holes”. In: 82.10, 104035 (Nov. 2010), p. 104035. DOI: 10.1103/PhysRevD.82.104035. arXiv: 1005.5605 [gr-qc].

[49] ESA. *Relativity and the 1919 eclipse*. URL: https://www.esa.int/Science_Exploration/Space_Science/Relativity_and_the_1919_eclipse.

[50] J. L. Synge. “The escape of photons from gravitationally intense stars”. In: 131 (Jan. 1966), p. 463. DOI: 10.1093/mnras/131.3.463.

[51] Ya B. Zel’dovich and Igor D. Novikov. “Reviews of Topical Problems: Relativistic Astrophysics. Ii”. In: *Soviet Physics Uspekhi* 8.4 (Apr. 1966), pp. 522–577. DOI: 10.1070/PU1966v008n04ABEH002990.

[52] Volker Perlick and Oleg Yu. Tsupko. “Calculating black hole shadows: Review of analytical studies”. In: 947 (Feb. 2022), pp. 1–39. DOI: 10.1016/j.physrep.2021.10.004. arXiv: 2105.07101 [gr-qc].

[53] Arne Grenzebach, Volker Perlick, and Claus Lämmerzahl. “Photon regions and shadows of Kerr-Newman-NUT black holes with a cosmological constant”. In: 89.12, 124004 (June 2014), p. 124004. DOI: 10.1103/PhysRevD.89.124004. arXiv: 1403.5234 [gr-qc].

[54] J. M. Bardeen. “Timelike and null geodesics in the Kerr metric.” In: *Black Holes (Les Astres Occlus)*. Jan. 1973, pp. 215–239.

[55] S. Chandrasekhar. *The Mathematical Theory of Black Holes*. Oxford University Press, 1992. ISBN: 9780198520504.

[56] Michael D. Johnson et al. "Universal interferometric signatures of a black hole's photon ring". In: *Science Advances* 6.12 (Mar. 2020), eaaz1310. DOI: 10.1126/sciadv.aaz1310. arXiv: 1907.04329 [astro-ph.IM].

[57] Brandon Carter. "Hamilton-Jacobi and Schrodinger Separable Solutions of Einstein's Equations". In: *Communications in Mathematical Physics* 10.4 (Dec. 1968), pp. 280–310. DOI: 10.1007/BF03399503.

[58] Rahul Kumar and Sushant G. Ghosh. "Black Hole Parameter Estimation from Its Shadow". In: 892.2, 78 (Apr. 2020), p. 78. DOI: 10.3847/1538-4357/ab77b0. arXiv: 1811.01260 [gr-qc].

[59] Leonardo Amarilla and Ernesto F. Eiroa. "Shadow of a rotating braneworld black hole". In: *Phys. Rev. D* 85 (6 2012), p. 064019. DOI: 10.1103/PhysRevD.85.064019. URL: https://link.aps.org/doi/10.1103/PhysRevD.85.064019.

[60] Kenta Hioki and Kei-ichi Maeda. "Measurement of the Kerr spin parameter by observation of a compact object's shadow". In: *Phys. Rev. D* 80 (2 2009), p. 024042. DOI: 10.1103/PhysRevD.80.024042. URL: https://link.aps.org/doi/10.1103/PhysRevD.80.024042.

[61] Marcus Bleicher et al. "Micro Black Holes in the Laboratory". In: *International Journal of Modern Physics E* 20 (Jan. 2011), pp. 7–14. DOI: 10.1142/S0218301311040529. arXiv: 1111.0657 [hep-th].